# An arms race between 5'ppp-RNA virus and its alternative recognition receptor MDA5 in RIG-I-lost teleost fish

Shang Geng[1], Xing Lv[1], Weiwei Zheng[1], Tianjun Xu[1,2,3,*]

1. *Laboratory of Fish Molecular Immunology, College of Fisheries and Life Science, Shanghai Ocean University, Shanghai, China*
2. *Laboratory for Marine Biology and Biotechnology, Qingdao Marine Science and Technology Center, Qingdao, China*
3. *Marine Biomedical Science and Technology Innovation Platform of Lin-gang Special Area, Shanghai, China*

*Corresponding author. Dr. Tianjun Xu

E-mail: tianjunxu@163.com

**Running title:** MDA5 recognizes 5'ppp-RNA virus in species lacking RIG-I

**Abstract:** The incessant arms race between viruses and hosts has led to numerous evolutionary innovations that shape life's evolution. During this process, the interactions between viral receptors and viruses have garnered significant interest since viral receptors are cell surface proteins exploited by viruses to initiate infection. Our study sheds light on the arms race between the MDA5 receptor and 5'ppp-RNA virus in a lower vertebrate fish, *M. miiuy*. Firstly, the frequent and independent loss events of RIG-I in vertebrates prompted us to search for alternative immune substitutes, with homology-dependent genetic compensation response (HDGCR) being the main pathway. Our further analysis suggested that MDA5 of *M. miiuy and G. gallus*, the homolog of RIG-I, can replace RIG-I in recognizing 5'ppp-RNA virus, which may lead to redundancy of RIG-I and loss from the species genome during evolution. Secondly, as an adversarial strategy, 5'ppp-RNA SCRV can utilize the $m^6A$ methylation mechanism to degrade MDA5 and weaken its antiviral immune ability, thus promoting its own replication and immune evasion. In summary, our study provides a snapshot into the interaction and coevolution between vertebrate and virus, offering valuable perspectives on the ecological and evolutionary factors that contribute to the diversity of the immune system.

**Keywords:** RIG-I; MDA5; 5'ppp-RNA; Genetic compensation response; Pattern recognition receptors; Immune evasion

## 1. Introduction

The Pattern recognition receptors (PRRs) recognize conserved pathogen-associated molecular pattern (PAMP) motifs, including proteins, lipids and nucleotides, resulting in activation of innate immune responses of host[1]. Retinoic acid-induced RIG-I-like receptors (RLRs) are a specific group of PRRs belonging to the family of DExD/H-box RNA helicases, and they play a crucial role in the innate antiviral response. There are three members in the RLR family: retinoic acid-inducible gene I (RIG-I), melanoma differentiation-associated gene 5 (MDA5), and laboratory of genetics and physiology 2 (LGP2). RIG-I and MDA5 exhibit similar signaling characteristics and structural homology, including two N-terminal caspase-recruitment domains (CARDs), a DExD/H box RNA helicase domain, and a C-terminal repressor domain (RD)[2]. However, LGP2 lacks CARD domain[2]. The specific roles of RIG-I and MDA5 in response to virus stimulation are not redundant: RIG-I detects short blunt-end RNA with a 5'-triphosphate motif (5’ppp-RNA), while MDA5 specifically recognizes long forms of viral dsRNA[3-5]. In contrast, the involvement of LGP2 in cytosolic RNA sensing remains a topic of debate. Some studies have proposed that LGP2 is crucial for the production of type I interferon (IFN-I) in response to several RIG-I- and MDA5-dependent viruses[6], whereas others have described LGP2 as a negative regulator of RIG-I signaling[7]. However, surprisingly, despite the important immune functions of RLR members, they have been lost from the genome in many species including mammals, birds, and fish[8-10].

5’ppp-RNA is present in a wide variety of RNA viruses, including Flaviviridae, Paramyxoviridae, Coronaviridae, Orthomyxoviridae, and Rhabdoviridae families[4]. These viruses widely infect all kinds of life and cause various harmfulness and serious diseases, and the infected

63 hosts range from the highest vertebrates to the lowest vertebrate, teleost fish [11, 12]. 5'ppp-RNA
64 viruses are expected to be recognized and trigger an antiviral immune response by RIG-I.
65 However, RIG-I is lacking in many vertebrates, so who then recognizes 5'ppp-RNA in these
66 species? When a gene is functionally inactive or lost, other genes or pathways may undergo
67 homology-dependent genetic compensation response (HDGCR) to maintain organismal balance.
68 The pressure from viral infections has led to the evolution of the immune system, and the loss of
69 RIG-I may be accompanied by functional substitution by homologous genes in order to
70 compensate for the loss of RIG-I function. *Tupaia belangeri*, a mammal lacking RIG-I, has been
71 reported to possess the MDA5 protein, which has undergone positive selection and exhibits the
72 ability to sense Sendai virus (an RNA virus posed as a RIG-I agonist) for inducing type I IFN[8].
73 This study provides insights into the compensatory mechanism of RIG-I deficiency in vertebrates,
74 however, considering the dynamic nature of host-virus dynamics, further research is urgently
75 needed to validate and expand these insights.

76 For millions of years, viruses have coevolved with their hosts, leading to the development of
77 various mechanisms for immune evasion in response to the mutual evolutionary pressure[13].
78 Recently, it is reported that N6-methyladenosine ($m^6A$) modification plays a crucial role in
79 enabling viruses to evade the interferon (IFN) response[14]. $m^6A$ methylation is an important
80 epigenetic modification that involves the dynamic and reversible process of RNA methylation,
81 regulated by methylase (writer), demethylase (eraser), and reader proteins that recognize $m^6A$-
82 modified RNA[15]. N6-methylation deposition on mRNA primarily relies on the enzymatic
83 "writing" complex within the cell, with a key composition featuring methyltransferase-like 3
84 (METTL3) and METTL14. Conversely, N6-demethylation is chiefly modulated by "eraser"

proteins, with fat mass and obesity-associated protein (FTO) and AlkB homolog 5 (ALKBH5) being the identified enzymes for this role [16,17]. The functional impact of N6-methylation on RNA characteristics typically remains latent until recognition by "reader" proteins, such as members of the YTHDF protein family, encompassing YTH domain family 1 (YTHDF1), YTHDF2, and YTHDF3. In mammals, YTHDF2 and YTHDF3 are recognized for their involvement in the degradation of $m^6A$-modified RNA targets, as well as their association with mRNA localization and phase separation [18]. By utilizing these $m^6A$-related enzymes in the host, viruses can not only use $m^6A$ modification to hide themselves and avoid recognition by host receptors but also manipulate host gene expression to enable immune evasion [19-21].

Fish and birds are commonly observed to exhibit "RIG-I deficiency" phenomena, and they are also the most abundant groups of aquatic and terrestrial vertebrates respectively, giving them certain evolutionary advantages. As a result, the research of the immune evolution of them helps us to understand the immune evolution of the entire vertebrates. Meanwhile, fish and birds are major source of high-quality protein for human consumption, viral diseases in aquaculture and livestock industry pose serious obstacles to the industry's healthy development. Among them, the 5’ppp-RNA virus, as mentioned earlier, is a highly pathogenic group. Within this group, *siniperca cheats* rhabdovirus (SCRV) is an important pathogen that can cause huge economic losses and serious threats to aquaculture in freshwater and marine fish [22]. In addition, vesicular stomatitis virus (VSV) is also a highly infectious and widely prevalent 5’ppp-RNA virus [12]. Therefore, in this study, we selected teleost fish miiuy croaker (*Miichthys miiuy*) and bird chicken (*Gallus gallus*), two vertebrates lacking RIG-I, as well as two 5'ppp-RNA viruses (SCRV and VSV), to investigate the evolutionary strategies and interactions between 5’ppp-RNA virus and host. The

final results demonstrated that the MDA5 of *M. miiuy* and *G. gallus* lacking RIG-I both evolved the ability to recognize 5'ppp-RNA. In addition, SCRV virus can in turn utilize the $m^6A$ strategy to degrade MDA5 of *M. miiuy* for immune evasion. In summary, these findings shed light on the functional diversity of innate antiviral activity and unveil a complex arms race between virus replication and the innate immunity of its reservoir hosts in vertebrates. In addition, since the loss of RIG-I in vertebrates is a widespread event, our research also provides a new perspective for vertebrate groups that have lost RIG-I.

## 2. Results

### *2.1 A genetic compensation response model for RIG loss*

In previous studies, it has been reported that a few vertebrates lost the RIG-I gene during evolution [9, 10, 23]. To investigate this further, we utilized the recent advancements in available and comprehensive genomic data of vertebrates from the NCBI and Ensemble websites. By analyzing the genomes of various species, we determined the presence and absence of the RIG-I gene. As depicted in Figure 1A, the absence of the RIG-I gene does not appear to be uncommon in vertebrates, with at least three independent loss events observed in mammals, birds and fish, respectively. These gene-loss events occurred over a long evolutionary timescale. Based on the minimum age of the common ancestor of RIG-I-missing species (http://www.timetree.org/), the oldest recorded losses occurring in species like *Erpetoichthys calabaricus*, can be traced back to approximately 330 million years ago (MYA). Conversely, the detected loss in *Gallus gallus* took place less than 42 MYA. To gain a deeper understanding of the evolutionary dynamics of vertebrate RIG-I, we explored the conservation of the genes surrounding RIG-I. We analyzed the genome sequences of *Homo sapiens*, *Callorhinchus milii*, *Danio rerio*, *Tupaia belangeri*, *Gallus gallus*, and *M. miiuy* (Figure 1B). Similar to the slow-evolving *Callorhinchus milii*, humans possess RIG-I with TOPORS and ACO1 as its upstream and downstream genes, respectively. As previously reported[8, 10]. *Tupaia belangeri*, *Gallus gallus*, and *M. miiuy* do not have RIG-I. Interestingly, zebrafish has a RIG-I with its upstream gene being TOPORSb, seemingly a result of chromosome fragment duplication. However, one RIG-I gene was lost in the downstream region of TOPORSa, indicating that one of the RIG-I copies has been lost in zebrafish, similar to *M. miiuy*.

137 Given the important role of RIG-I in recognizing 5'ppp RNA, we selected two different
138 models for experiments to detect the presence of other potential receptors for immune
139 compensation in RIG-I deficient species. Specifically, we extracted virus RNA from SCRV and
140 VSV viruses and obtained their dephosphorylated RNA derivatives (SCRV-RNA-CIAP and VSV-
141 RNA-CIAP) through Calf Intestinal Alkaline Phosphatase (CIAP) treatment. Next, these RNAs
142 were transfected into MKC cells of *M. miiuy* and DF-1 cells of *G. gallus* respectively to detect the
143 dimerization form of IRF3. Results showed that virus RNA are more potent than dephosphorylated
144 virus RNA in activating IRF3 (Figure 1C and 1D). And further qPCR experiments showed that the
145 induction ability of IFN-1 by SCRV-RNA is significantly higher than that of SCRV-RNA-CIAP.
146 These results indicate the presence of viral receptors in *M. miiuy* and *G. gallus* that can recognize
147 5’ppp-RNA. Next, we compared the structural domains of human RIG-I and *M. miiuy* MDA5
148 (mmiMDA5) and LGP2 (mmiLGP2) proteins, and observed that mmiLGP2 lacks the CARD
149 domain (Figure 1F). We next constructed the mmiLGP2 plasmid and synthesized siRNA targeting
150 mmiLGP2, and co-transfected them with MDA5 plasmids into MKC cells. The results showed
151 that mmiLGP2 can actively regulate mmiMDA5's immune response to the SCRV virus (Figure 1H
152 and 1I), which further indicates that it participates in antiviral immunity as an intermediate
153 regulatory factor of MDA5 rather than a downstream signal transmitter[7]. Therefore, these results
154 prompted us to investigate whether MDA5, a structurally similar homolog to RIG-I, can substitute
155 for RIG-I in recognizing 5'ppp-RNA in vertebrates without RIG-I (Figure 1J).
156
157 ***2.2 MDA5 promotes host antiviral innate immunity***

158 To further investigate the alternative immune function of MDA5, we first investigated the *M.*
159 *miiuy* MDA5-mediated signaling pathway in response to SCRV virus and double-stranded
160 mimetic poly(I:C)-HMW infection. Two siRNA molecules (si-MDA5-1 and si-MDA5-2) were
161 designed to assess the function of MDA5. si-MDA5-1 demonstrated higher inhibitory efficiency
162 compared to si-MDA5-2 (Figure 2A). Therefore, si-MDA5-1 (referred to as si-MDA5) was
163 selected for subsequent experiments. Subsequently, we constructed the MDA5 expression plasmid
164 and confirmed its protein overexpression efficiency and cytoplasmic localization (Figure 2B and
165 2C). Considering that mammalian MDA5 activates NF-κB and IRF3/IRF7 to induce IFNs, we
166 investigated whether *M. miiuy* MDA5 could impact these pathways. Dual-luciferase reporter
167 assays demonstrated that knockdown of MDA5 significantly inhibits NF-κB, IRF3, IRF7, and
168 IFN-1 reporter genes (Figure 2D). In addition, we investigated the role of MDA5 in regulating the
169 expression of IFN-stimulated genes (ISGs), which are crucial effectors. As shown in Figure 2E-
170 2G, we observed that knockdown or overexpression of MDA5 can significantly inhibit or promote
171 the expression levels of IFN-1, Mx1, ISG15, and Viperin upon SCRV infection or poly(I:C)-HMW
172 stimulation. To visually represent the biological significance of MDA5 in SCRV-induced host
173 cells, we utilized the virus plaque and qPCR methods to examine whether it could influence viral
174 replication. As demonstrated in Figure 2H-2K, knockdown of MDA5 led to a significant increase
175 in viral plaque formation and promoted SCRV replication in SCRV-infected cells, while
176 overexpression had the opposite effect. Next, we explored that how MDA5 conducts signal
177 transduction, and results showed that MDA5 is capable of binding not only to MAVS but also to
178 STING (Figure 2L and 2M). Under the infection of SCRV virus, co-transfection of STING
179 plasmids or si-STING with MDA5 plasmids can significantly increase or decrease the induction of

180 IFN-1, indicating the important role of STING in MDA5-mediated immune transmission in
181 response to RNA virus (Figure 2N and 2O). Finally, through the determination of IRF3 dimer and
182 IFN induction, our results showed that the induction of antiviral innate immunity by SCRV-RNA
183 depends on MDA5 (Figure 2P and 2Q). Overall, these findings indicated that MDA5 plays a
184 positive role in regulating the antiviral responses of *M. miiuy*.
185
186 ***2.3 RD domain is required for MDA5 to recognize SCRV RNA***
187 We investigated whether *M. miiuy* MDA5, in the absence of RIG-I, can directly bind to the
188 RNA of SCRV. To address this question, we precipitated the MDA5 protein from SCRV-infected
189 MKC cells that were transfected with MDA5-Flag and pcDNA3.1-Flag. The bound RNA was then
190 amplified using SCRV-specific primers or β-actin primers as a control. Our results showed that
191 MDA5 interacted with SCRV RNA, while β-actin mRNA did not associate with MDA5 (Figure
192 3A). The C-terminal regulatory domain (RD) of human RIG-I binds to viral RNA in a
193 triphosphate-dependent manner, to determine if the RD domain of *M. miiuy* MDA5 has similar
194 functions, we generated truncated mutations called MDA5-ΔRD and Western blot analysis
195 confirmed the expression of MDA5 and MDA5-ΔRD plasmids (Figure 3B). We subsequently
196 noted that MDA5-ΔRD exhibited an inability to interact with SCRV RNA, which was supported
197 by the loss of its immunological capability in inhibiting SCRV viral replication (Figure 3C-3E).
198 We also examined the effects of MDA5 and its mutant on antiviral factors in both poly(I:C)-
199 HMW-stimulated and SCRV-infected MKC cells. Results showed that only the overexpression of
200 MDA5, not MDA5-ΔRD, significantly increased the expression of antiviral genes (Figure 3F and

201 3G). In summary, these findings provided evidence that MDA5 may recognize 5’ppp-RNA
202 through its RD domain.
203
204 ***2.4 MDA5 recognizes 5’ppp-RNA in M. miiuy and G. gallus***
205 To provide specific evidence of MDA5 recognition of 5’ppp-RNA in *M. miiuy*, we
206 synthesized 67 nt 5’ppp-SCRV from the SCRV virus and through in vitro transcription using T7
207 polymerase. As a positive control capable of binding to the mmiMDA5 receptor, 112 bp dsRNA
208 from the MDA5 gene sequence was also generated. Gel analysis and nuclease sensitivity
209 confirmed the generation of RNA products of the expected size (Figure 4A). The RNA pull-down
210 experiment showed that 5’ppp-SCRV can be recognized by mmiMDA5, similar to 112 bp blunt
211 end dsRNA (Figure 4B). Next, we transfected wild-type 5’ppp-SCRV and dephosphorylated
212 mutant SCRV RNAs (5’-OH-SCRV and 5’pppGG-SCRV) into MKC cells to detect the dimer of
213 IRF3, and found that the activation ability of 5'ppp-RNA on IRF3 depends on its triphosphate
214 structure (Figure 4C). Furthermore, biotin-labeled 5’ppp-RNA captured mmiMDA5, while the
215 biotin-labeled mutant types (5’-OH-SCRV and 5’pppGG-SCRV) did not (Figure 4D).
216 Additionally, we purified recombinant MDA5 and MDA5-ΔRD of *M. miiuy* to conduct
217 electrophoresis mobility shift assay (EMSA) (Figure 4E). When recombinant mmiMDA5 was
218 subjected to EMSA using a biotin-labeled 5’ppp-SCRV probe, a clear complex was detected
219 (Figure 4F). This complex formation was inhibited by adding an excess of cold 5’ppp-SCRV but
220 not 5’-OH-SCRV and 5’pppGG-SCRV, demonstrating the direct interaction between mmiMDA5
221 and 5’ppp-SCRV (Figure 4F). However, 5’ppp-SCRV cannot bind to the MDA5-ΔRD (Figure
222 4G). Next, we investigated whether *G. gallus* MDA5 (ggaMDA5) shares the ability to recognize

223 5’ppp-RNA seen in fish. We synthesized 67 nt 5’ppp-VSV from the VSV virus and found that it is
224 similar to 5’ppp-SCRV, binding to ggaMDA5 and activating IRF3 in a triphosphate-dependent
225 manner (4H-4L). Overall, our findings demonstrated that MDA5 detection of RNA in two RIG-I
226 deficient vertebrates (*M. miiuy and G. gallus*) is guided by the RNA 5'-triphosphate end and is
227 disrupted when RNA is capped at the 5'-triphosphate end or dephosphorylated.
228

229 ***2.5 Increased m$^6$A modification and expression of MDA5 upon SCRV infection***

230 As stated in the previous results, MDA5 has evolved to possess immune recognition abilities
231 that take over the role of RIG-I, significantly enhancing the host's ability to resist viral infections.
232 However, evolution is a continuous battle between hosts and viruses, viruses often evolve complex
233 escape mechanisms to evade immune surveillance and destruction, in which the m$^6$A modification
234 mechanism is an important way. To investigate the impact of SCRV infection on the overall
235 methylation dynamics of fish hosts, we utilized methylated RNA immunoprecipitation sequencing
236 (MeRIP-seq, GenBank accession number: PRJNA819945) to measure changes in m$^6$A
237 modification of host transcripts during SCRV infection (Figure 5A). From the results shown in
238 Figure 5B, we identified 3060 differentially m$^6$A methylated peaks ($p$-value < 0.05) and 2082
239 differentially expressed genes ($p$-value < 0.05) between the non-infected and SCRV-infected
240 group, indicating that infection significantly alters the m$^6$A modification of specific host
241 transcripts. It is worth noting that hyper-methylated m$^6$A peaks were also observed in the MDA5
242 mRNA transcripts during SCRV infection (fold change >1.5, $p < 0.05$), and the expression level of
243 MDA5 was higher in the infection group compared to the control group ($p < 0.05$). Further
244 analysis of the m$^6$A-seq data showed that MDA5 contained m$^6$A sites in the exon1 region which

245 were markedly higher in the infection group than that in the control group (Untreated VS SCRV: $p$
246 = 0.01) (Figure 5C). Next, we tested the concrete m$^6$A modification sites of MDA5 mRNA. We
247 used the SRAMP database to predict potential m$^6$A sites in MDA5-exon1 [24]. Four potential sites
248 were predicted and two specific primers were designed (Figure 5D), then m$^6$A quantitative real-
249 time PCR and semiquantitative PCR were performed. In line with the m$^6$A-seq data, the results
250 further confirmed that m$^6$A sites exactly exist in MDA5 exon1 (Figure 5E). After being infected
251 with SCRV or poly(I:C)-HMW, the methylation level of MDA5 increased in MKC cells, further
252 confirming the sequencing data (Figure 5F). Next, MDA5 was found to be upregulated in spleen
253 and kidney tissues infected with SCRV (Figure 5G). We further explored the mRNA and protein
254 levels of MDA5 in MKC cells infected with SCRV and poly(I:C)-HMW and found that their
255 expression all first significantly increased and then returned to the normal level (Figure 5H and
256 5I). Overall, our results suggested that both the m$^6$A modification and expression levels of MDA5
257 are increased upon SCRV infection.
258
259 ***2.6 m$^6$A-modification weakens MDA5 mRNA stability and antiviral ability***
260 SCRV infection can increase the methylation level of MDA5, and this mechanism is expected
261 to have a regulatory effect on MDA5. To investigate this, the regulatory effects of METTL3 and
262 METTL14, the main components of the methyltransferase complex, on MDA5 were explored.
263 Three siRNAs targeting METTL3 and METTL14 were designed, and si-METTL3-2 and si-
264 METTL14-3 showed higher knockdown efficiency (Figure 6A). METTL3 and METTL14-
265 overexpressing plasmids were also constructed, and the interaction between them confirmed their
266 cooperative role in m$^6$A modification (Figure 6B). Subsequently, the global m$^6$A levels were

measured in cells after knockdown or overexpression of METTL3 and METTL14. Consistent with expectations, the knockdown of METTL3 and METTL14 significantly decreased the global $m^6A$ level, while their overexpression significantly increased the overall methylation level (Figure 6C). To investigate their role in the process of virus infection, we used the virus plaque and qPCR methods to explore whether it could affect SCRV replication. As shown in Figure 6D and 6E, overexpression of METTL3 or METTL14 significantly enhances viral plaque formation and promotes SCRV replication in SCRV-infected cells. And as $m^6A$ writers, METTL3 and METTL14 can directly regulate the methylation level of MDA5 and induce MDA5 degradation by reducing its mRNA stability (Figure 6F-6I). We further inserted the MDA5-exon1 into pmirGLO and mVenus-C1 vector, and results showed that si-METTL3&14 can reduce the luciferase activity of pmirGLO-MDA5-exon1, and METTL3&14 could suppress the levels of GFP, further indicating the presence of methylation sites in MDA5-exon1 (Figure 6-figure supplement 1A and 1D). To investigate the potential sites on MDA5-exon1, we constructed mutant MDA5-exon1 reporter plasmids. For the mutant form of MDA5-exon1 reporter genes, four predicted adenosine bases in $m^6A$ consensus sequences (DRACH) were replaced by uracil, thus canceling $m^6A$ decoration (Figure 5D and Figure 6-figure supplement 1B). As expected, our results showed that the luciferase activity of wild-type pmirGLO-MDA5-exon1 reporter, but not of mutant pmirGLO-MDA5-exon1 reporter, was markedly increased upon METTL3&14 knockdown (Figure 6-figure supplement 1C). Furthermore, we found that the use of cycloleucine (CL, an amino acid analogue that can inhibit $m^6A$ modification) hindered the degradation of MDA5 by METTL3 and METTL14, indicating that these proteins regulate MDA5 expression through a methylation mechanism (Figure 6J and 6K). Additionally, MDA5 expression was degraded by METTL3&14 in

289 both SCRV-infected and uninfected groups (Figure 6L). To investigate the impact of this
290 mechanism on viral infection, we co-transfected METTL3&14 and MDA5 plasmids and found
291 that METTL3&14 partially suppressed the antiviral immune benefit of MDA5 (Figure 6M-6O).
292 Taken together, our data demonstrate that METTL3&14-mediated $m^6A$ methylation of MDA5
293 inhibits its mRNA stability and expression levels, thus suppressing the antiviral capabilities of
294 MDA5.
295
296 ***2.7 Detailed $m^6A$ regulatory mechanism of MDA5***
297 The $m^6A$ mechanism is jointly regulated by writers, erasers, and readers. The $m^6A$
298 modification of mRNA recruits $m^6A$-binding proteins (readers) which have the function of
299 recognizing $m^6A$ sites and accelerating mRNA decay. In this study, we hypothesized that YTHDF
300 readers (YTHDF1, YTHDF2, and YTHDF3) may recognize $m^6A$-modified MDA5 and destabilize
301 it. We examined the binding ability of YTHDF proteins to MDA5 mRNA and found that YTHDF2
302 and YTHDF3 exhibited stronger binding compared to YTHDF1 (Figure 7A). We then designed
303 two siRNAs targeting YTHDF1, YTHDF2, and YTHDF3 respectively, and selected si-YTHDF1-
304 1, si-YTHDF2-si-2, si-YTHDF3-2 with better knockdown effects for subsequent experiments
305 (Figure 7B). Results showed that the knockdown or overexpression of YTHDF2 and YTHDF3 led
306 to the increase or decrease of the expression levels of MDA5, whereas YTHDF1 did not appear to
307 influence MDA5 expression (Figure 7C, 7D, Figure 7-figure supplement 1A and 1C). In addition,
308 overexpression of YTHDF2&3 can increase the luciferase activity of wild-type pmirGLO-MDA5-
309 exon1 reporter, but not of mutant pmirGLO-MDA5-exon1 reporter (Figure 7-figure supplement
310 1B). We then found that si-METTL3&14 can counteract the negative impact of YTHDF2&3 on

311 MDA5 mRNA, protein, and stability (Figure 7E and 7F). Since the $m^6A$ mechanism is reversible,
312 we then studied the regulation of MDA5 by two major erasers. Results showed that FTO, not
313 ALKBH5, can upregulate MDA5 expression (Figure 7G). Moreover, the overexpression of FTO
314 can reverse the inhibitory effect of YTHDF2&3 on MDA5 (Figure 7H and 7I). Taken together,
315 these data suggested that through METTL3&14-$m^6A$-YTHDF2&3 regulatory network, $m^6A$ can
316 mediate the degradation of MDA5, and this process can be countered by FTO (Figure 7J).
317

318 **3. Discussion**

319 In this study, we have identified multiple independent loss events of RIG-I throughout
320 vertebrate evolution. Specifically, we have observed at least three independent loss events in
321 mammals, birds, and fish, respectively. Regarding the loss of RIG-I in avian species, previous
322 studies have provided more comprehensive and accurate information than ours, indicating that
323 birds have experienced more than 16 instances of RIG-I loss[10]. However, it should be noted that
324 we have not found the loss of RIG-I in reptiles and amphibians (not displayed). But this does not
325 imply that there has been no loss event among them, but rather, there is insufficient information
326 regarding the genomes of reptiles and amphibians to draw the conclusions. As the abundance of
327 genomic data continues to grow, there will be an increasing amount of evidence available to verify
328 the presence or absence of RIG-I in these taxonomic groups. Additionally, the presence of RIG-I
329 in current species does not guarantee that RIG-I loss has not occurred previously. For instance, our
330 research has indicated that zebrafish may have experienced RIG-I loss. However, prior to the loss
331 event, the zebrafish RIG-I has undergone repetitive events. These findings collectively highlight
332 that the loss of RIG-I is not a random occurrence, but rather bears significant biological and
333 evolutionary implications that deserve further investigation.

334 The loss of RIG-I might be expected to have a great impact on immune response, and the
335 evolutionary loss of it raises the question of a possible compensation of its function by other gene
336 products. RIG-I deficiency instances in mammals were scarcer compared to those in fish and
337 birds. Previous research has revealed that in *T. belangeri*, concurrent with the loss of RIG-I, both
338 MDA5 and LGP2 have undergone notable positive selection, and MDA5 or MDA5/LGP2 could
339 sense Sendai virus (an RNA virus posed as a RIG-I agonist) for inducing type I IFN. This

340 proposed an immune substitution model for RIG-I deficiency in mammals, though direct evidence
341 of MDA5/LGP2 binding to 5'ppp-RNA was lacking. In this study, we characterized the
342 consequences resulting from the loss of RIG-I in the *M. miiuy* and *G. gallus* (two representative
343 species of vertebrates lacking RIG-I) and provided direct functional evidence for the alternative
344 immune recognition function of MDA5. SCRV and VSV belongs to the class of rhabdovirus,
345 which is a negative-strand virus with a non-segmented genome and initiate both replication and
346 transcription de novo leading to 5′-triphosphate RNA in the cytosol, was expected to trigger an
347 IFN response without the need for replication and presumed dsRNA formation[4]. Then, we
348 synthesized 5'ppp-RNA probes from the SCRV and VSV genome sequences and purified
349 recombinant MDA5 of *M. miiuy* and *G. gallus*. Results demonstrated that MDA5 detect the 5'ppp-
350 RNA in *M. miiuy and G. gallus* and is disrupted when RNA is capped at the 5'-triphosphate end or
351 dephosphorylated. Furthermore, the recognition of RNA by MDA5 depends on its RD domain,
352 which not only indicates that the RD domain of MDA5 has evolved functions similar to RD
353 domain of RIG-I, but also excludes the possibility of MDA5 binding to 5'ppp-RNA through
354 intermediate ligands. Furthermore, in vertebrates that possess RIG-I, STING exclusively binds to
355 RIG-I rather than MDA5. However, similar to the interaction observed between MDA5 and
356 STING in tree shrews and chickens that lacking RIG-I[8, 25], the MDA5 of *M. miiuy* can also interact
357 with STING protein, indicating that in vertebrates lacking RIG-I, MDA5 may utilize STING to
358 facilitate signal transduction in the antiviral response. Finally, by linking the immune replacement
359 ability evolved by MDA5 with the common RIG-I loss event in vertebrates, we propose a
360 straightforward explanation for this evolutionary event: In the lengthy process of vertebrate
361 evolution, MDA5 gradually acquired new functionalities to effectively detect viruses such as

362 5'ppp-RNAs, which were initially recognized by RIG-I. As a result, there was functional
363 redundancy of RIG-I, which eventually led to its gradual disappearance from the vertebrate
364 genome. This hypothesis is supported by two viewpoints: first, MDA5 and RIG-I can both
365 recognize overlapping viruses[26]; secondly, in fish without RIG-I deficiency, MDA5 has stronger
366 antiviral ability compared to RIG-I[27].

367 Viruses are constantly co-evolving with hosts. Our available data suggested that the
368 vertebrate has evolved MDA5 with alternative functions to recognize and resist 5'ppp-RNA virus
369 in the absence of RIG-I. As a response, virus has also evolved to use the $m^6A$ mechanism to evade
370 the host immune response. Previous study indicated that $m^6A$ modification plays a crucial role in
371 maintaining immune homeostasis in the body[28]. During the infection process, the virus may
372 disrupt the $m^6A$ level and disrupt the immune balance, thereby facilitating its own replication and
373 invasion. Viruses may utilize the $m^6A$ mechanism in two ways to evade immunity. On the one
374 hand, many studies suggested a role for $m^6A$ in shielding RNA species from detection by PRRs.
375 There are numerous viruses recognized in RIG-I dependent manner, but $m^6A$ modification
376 increases the possibility of immune evasion. For example, the loss of $m^6A$ site or removing $m^6A$
377 from human metapneumovirus may weaken its immune evasion ability, prevent it from evading
378 detection by RIG-I, and result in higher levels of IFN release[20]. Moreover, it has been reported
379 that the RNA containing $m^6A$ modifications binds to RIG-I poorly, and it failed to trigger the RIG-
380 I conformational changes associated with downstream immune signals[29]. On the other hand, $m^6A$-
381 mediated viral strategies for inhibiting IFN induction pathways appear to exist. For instance,
382 following infection by human cytomegalovirus (HCMV), the IFN-β transcript was modified by
383 $m^6A$, and this methylation decreased its half-life, suggesting that HCMV can exploit this control

384 of IFN-β expression to facilitate its replication by increasing $m^6A$ modification of the IFN-β
385 transcript and thus decreasing its production[30]. In another study, the m6A reader YTHDF3 could
386 restrain the type I IFN response and ISG expression by involving enhancement of FOXO3
387 translation in a m6A-independent mechanism, which acts as a negative regulator of immunity [19].
388 Moreover, previous study reports that IFN-α and IFN-β mRNA encoding cytokines that promote
389 IFN response are modified by m6A, and the loss of METTL3 and YTHDF2 could increase the
390 IFN expression and ISG activity [31]. In summary, viruses can utilize $m^6A$ to evade the immune
391 response by shielding the recognition of RIG-I or reducing the host's immune reaction, thus
392 counteracting the host's defense mechanisms. In our previous study, we discovered that SCRV
393 infection can not only increase overall cellular methylation levels but also upregulate the
394 expression of METTL3, thereby suggesting its potential to regulate host gene expression through
395 the $m^6A$ mechanism[32]. In this study, we found that SCRV virus infection alters $m^6A$ modification
396 of specific cellular transcripts, including MDA5. MDA5 plays a crucial role as a receptor in
397 recognizing the SCRV virus and controlling IFN activation. The aberrant $m^6A$ levels of MDA5
398 subsequently affect the expression of antiviral genes, thereby compromising its ability to mount an
399 effective antiviral immune response. It is plausible that SCRV also impacts the production of
400 antiviral genes, such as IFN-1 or other cytokines, by manipulating $m^6A$ modification on the
401 transcripts of cytokines or molecules involved in their production. This interesting aspect warrants
402 further investigation in future research.

403 In this study, we demonstrated a co-evolutionary arms race between 5'ppp-RNA virus and
404 virus receptors. Specifically, we conducted an evolutionary analysis and provided functional
405 evidence to confirm that MDA5 of *M. miiuy* and *G. gallus* has acquired an additional function of

406 sensing 5'ppp-RNA, thus compensating for the loss of RIG-I. Additionally, we found that SCRV
407 infection can regulate the $m^6A$ level of MDA5 in the *M. miiuy*, leading to its degradation and
408 subsequently affecting the immune response for immune evasion. Fish and birds, as the most
409 abundant aquatic and terrestrial vertebrates respectively, are also the two lineages with the most
410 frequent occurrence of RIG-I deficiency, the investigation of host-pathogen interactions of them
411 offers valuable insights into the ecological and evolutionary factors that contribute to the diversity
412 of the immune system.
413

414 ## 4. Materials and methods

415 ### *4.1 Ethics statement*

416 All animal experimental procedures were performed in accordance with the National
417 Institutes of Health's Guide for the Care and Use of Laboratory Animals, and the experimental
418 protocols were approved by the Research Ethics Committee of Shanghai Ocean University (No.
419 SHOU-DW-2018-047).

420

421 ### *4.2 Fish and challenge*

422 *M. miiuy* (~50 g) was obtained from Zhoushan Fisheries Research Institute, Zhejiang
423 Province, China. Fish was acclimated in aerated seawater tanks at 25℃ for six weeks before
424 experiments. The experimental procedure for SCRV infection was performed as described[33].
425 Briefly, In the SCRV injection group, fish was challenged with 200 μl SCRV at a multiplicity of
426 infection (MOI) of 5 through intraperitoneal. As a comparison, 200 μl of physiological saline was
427 used to challenge the individuals. Afterwards, fishes were respectively sacrificed at different time
428 point and the kidney and spleen tissues were collected for RNA extraction.

429

430 ### *4.3 Cell culture and treatment*

431 *M. miiuy* kidney cells (MKCs) and spleen cells (MPCs) are cell lines derived from the
432 kidney and spleen tissues of *M. miiuy* [34], with passages ranging from 20 to 40 times. MKC and
433 MPC cells were cultured in L-15 medium (HyClone) supplemented with 15% fetal bovine serum
434 (FBS; Gibco), 100 U/ml penicillin, and 100 μg/ml streptomycin at 26℃. Fish EPC cells
435 (Epithelioma papulosum cyprini cells) were maintained in medium 199 (Invitrogen) supplemented

436 with 10% FBS, 100 U/ml penicillin, and 100 mg/ml streptomycin at 26℃ in 5% $CO_2$. HEK293T
437 cells were cultured in DMEM (HyClone) supplemented with 10% FBS, 100 U/ml penicillin, and
438 100 mg/ml streptomycin at 37℃ in 5% $CO_2$. Chicken embryo fibroblast cells (DF-1) were
439 cultured in DMEM (HyClone) supplemented with 10% FBS, 100 U/ml penicillin, and 100 mg/ml
440 streptomycin at 39℃ in 5% $CO_2$. For stimulation experiments, cells were challenged with SCRV
441 at a multiplicity of infection (MOI) of 5 and harvested at different times for RNA extraction.
442
443 ***4.4 Oligonucleotides***
444 The sequence of the 62 nt 5'ppp-RNA was derived from the 5' and 3'UTRs of the VSV
445 genome as previously described[37], and the sequence of 112 bp dsRNA was taken from the first 100
446 bp of the MDA5 gene of miiuy croaker flanked by 5'-gggaga and tctccc-3'. 67 nt 5'ppp-SCRV or
447 5'ppp-VSV and 112 bp dsRNA were synthesized by in vitro transcription using the Ribo
448 RNAmax-T7 kit (RiboBio). Biotin-labeled RNAs were transcribed in vitro using a Ribo
449 RNAmax-T7 Biotin Labeling Transcription Kit (RiboBio). For generating duplexes, RNA
450 oligonucleotides were mixed in hybridization buffer (20 mM Tris-HCl [pH 8.0], 1.5 mM $MgCl_2$,
451 and 1.5 mM DTT), boiled for 1 min, and incubated at 37℃ for 1 h. For removal of 5'-
452 triphosphates, 20 mg of RNA was treated with 20 U Calf Intestinal Alkaline Phosphatase (CIAP,
453 Invitrogen) for 2 h at 37℃ in the presence of RNase inhibitor (Beyotime) and extracted with
454 phenolchloroform. RNA molecules with a terminal 5' m7G cap were synthesized by the
455 incorporation of m7G cap analogue (Yeason) in the transcription reactions. RNA was analysed on
456 a denaturing 17% polyacrylamide, 7 M urea gel following digestion with 50 ng/μl of RNase A
457 (Beyotime) or 100 mU/μl of DNase I (Beyotime) for 30 min.

458

459 ***4.5 Plasmids construction***

460 To construct Flag or Myc-tagged MDA5 (GeneBank: PP179381.1), MAVS, STING,
461 METTL3, METTL14, FTO, ALKBH5, YTHDF1, YTHDF2, and YTHDF3 expression plasmids,
462 their CDS sequences of the *M. miiuy* were amplified by PCR and then ligated into a pcDNA3.1
463 vector (Invitrogen), respectively. Then, MDA5-△RD were generated by PCR on the basis of
464 MDA5 plasmid. To construct MDA5-exon1 reporter vector, the exon1 region of *M. miiuy* MDA5
465 gene was amplified using PCR with the gene-specific primers and ligated into a pmir-GLO
466 luciferase reporter vector (Promega). Meanwhile, *M. miiuy* MDA5-exon1 were inserted into the
467 mVenus-C1 (Invitrogen), which included the sequence of enhanced GFP. For mutant reporter
468 vectors (MDA5-exon1-mut), adenosine (A) in the predicted $m^6A$ motif was replaced by an uracil
469 (U) by using the Mut Express II Fast Mutagenesis Kit V2 (Vazyme) with specific primers). To
470 construct Flag-tagged MDA5 expression plasmid of *G. gallus*, the CDS sequence of MDA5 was
471 amplified by PCR and then ligated into a pcDNA3.1 vector (Invitrogen). The correct construction
472 of the recombinant plasmids was verified through Sanger sequencing and extracted using an
473 Endotoxin-Free Plasmid DNA Miniprep Kit (Tiangen, China) before using plasmids. The primers
474 were listed in Supplementary file 1.

475

476 ***4.6 Protein Purification and Analysis***

477 For protein purification, MDA5 plasmids with 6× His tag was constructed based on
478 pcDNA3.1. (His6)-Flag-tagged MDA5 of *M. miiuy* and *G. gallus* were transiently overexpressed
479 in 293T cells and lysed in a binding buffer (500 mM NaCl, 20 mM Tris/HCl [pH 7.4], 20 mM

480 Imidazole, and 1% Triton X-100) including protease inhibitor cocktail (Roche). The lysate was
481 incubated over night at 4℃ with anti-His beads (Solarbio). Anti-His beads were washed
482 subsequently with washing buffer (500 mM NaCl, 20 mM Tris/HCl [pH 7.4], 20 mM Imidazole,
483 and 1% Triton X-100). MDA5 proteins were eluted by an addtion of elution buffer (500 mM
484 NaCl, 20 mM Tris/HCl [pH 7.4], 500 mM Imidazole, and 1% Triton X-100) to the beads. Purity of
485 recombinant MDA5 was determined by SDS-PAGE separation.
486
487 ***4.7 RNA interference***
488 The MDA5-specific small interfering RNA (si-MDA5-1 and si-MDA5-2) sequences were 5'-
489 CGGACUACAUGCAGCGUAATT-3' and 5'-GACCAAUGAGAUUUCUAUGTT-3',
490 respectively. The LGP2-specific small interfering RNA (si-LGP2) sequence was 5'-
491 GGUUCACCUUGUAGAGCAATT-3'. The STING-specific small interfering RNA (si-STING)
492 sequence was 5'-ACGACAGCAUCCAUUUCUATT-3'. The METTL3-specific small interfering
493 RNA (si-METTL3-1, si-METTL3-2, and si-METTL3-3) sequences were 5'-
494 CAUCACAAACGAACUCAACTT-3', 5'- AACGUGGGCAAACUCUUUUTT-3' and 5'-
495 GAGAUUCUGGAACUACUUATT-3', respectively. The METTL14-specific small interfering
496 RNA (si-METTL14-1, si-METTL14-2, and si-METTL14-3) sequences were 5'-
497 GCUGGAAAUCGAGGAGAUATT-3', 5'- CCGTACGAAGAGGTGTACATT-3' and 5'-
498 GAGCCUCCCUUGGAAGAAUTT-3', respectively. The YTHDF1-specific small interfering
499 RNA (si-YTHDF1-1 and si-YTHDF1-2) sequences were 5'-AAAGACUUUGACUGGAACUTT-
500 3' and 5'-CAGUCGAUCAGAGACCUAATT-3', respectively. The YTHDF2-specific small
501 interfering RNA (si-YTHDF2-1 and si-YTHDF2-2) sequences were 5'-

502 GCAGGGUGUUUAUCAUCAATT-3', 5'- CUAUGCUCCCAGCUCAAUUTT-3', respectively.
503 The YTHDF3-specific small interfering RNA (si-YTHDF3-1 and si-YTHDF3-2) sequences were
504 5'-GGUGGACUACAAUGCCUAUTT-3' and 5'-UCUACAGUAACAGCUAUGGTT-3',
505 respectively. The scrambled control RNA sequences were 5' - UUCUCCGAACGUGUCACGUTT
506 - 3'. They were purchased from GenePharma (Shanghai, China).
507

508 ***4.8 Cells transfection***

509 Transient transfection of cells with siRNA was performed in 24-well plates using
510 Lipofectamine RNAiMAX (Invitrogen), and cells were transfected with DNA plasmids was
511 performed using Lipofectamine 3000 (Invitrogen) according to the manufacturer's instructions.
512 For functional analyses, the overexpression plasmid (500 ng per well) or control vector (500 ng
513 per well) and siRNA (100 nM) were transfected into cells in culture medium and then harvested
514 for further detection.
515

516 ***4.9 RNA extraction and quantitative real-time PCR***

517 Total RNA was extracted using the TRIzol Reagent (Invitrogen) and the cDNA was
518 synthesized using the FastQuant RT Kit (Tiangen) which contains DNase treatment of RNA to
519 eliminate genomic contamination, following the manufacturer's instructions. The expression
520 profiles of each gene were conducted by using the SYBR Premix Ex Taq™ (Takara), as
521 previously described. The quantitative real-time PCR was conducted in an Applied Biosystems®
522 QuantStudio 3 (Thermo Fisher Scientific). β-actin was used as internal controls for mRNA
523 respectively. Primer sequences are listed in Supplementary file 1.

524

525 ***4.10 Western blotting***

526 Cellular lysates were generated by using 1×SDS-PAGE loading buffer. Proteins were
527 extracted from cells and measured with the BCA Protein Assay kit (Vazyme), then subjected to
528 SDS-PAGE (10%) gel and transferred to PVDF (Millipore) membranes by semidry blotting (Bio-
529 Rad Trans Blot Turbo System). The membranes were blocked with 5% BSA. Protein was blotted
530 with different antibodies. The antibody against MDA5 was diluted at 1: 500 (Beyotime, Cat#
531 AF7164); The antibody against IRF3 was diluted at 1: 500 (Boster, Cat# BA4351-2); anti-Flag,
532 anti-Myc, anti-HA and anti-Tubulin monoclonal antibody were diluted at 1: 1,000 (Beyotime);
533 and HRP-conjugated anti-rabbit IgG or anti-mouse IgG (Abbkine) at 1: 5,000. The results were
534 the representative of three independent experiments. The immunoreactive proteins were detected
535 by using WesternBright$^{TM}$ ECL (Advansta). The digital imaging was performed with a cold CCD
536 camera.

537

538 ***4.11 Dual-luciferase reporter assays***

539 To determine the functional regulation of MDA5, MKC cells were co-transfected MDA5
540 expression plasmid, together with NF-κB, IRF3, IRF7, or IFN-1 luciferase reporter genes, and the
541 pRL-TK *Renilla* luciferase reporter plasmid. After 48 h transfection, the cells were collected and
542 lysed for reporter activity using the dual-luciferase reporter assay system (Promega). For the
543 detection of $m^6A$ site, the wild or mutant of MDA5-exon1 luciferase reporter was co-transfected
544 si-METTL3, si-METTL14, si-YTHDF1, si-YTHDF2, si-YTHDF3 or si-Ctrl into MKC cells. After
545 48 h transfection, the cells were collected and lysed for the reporter luciferase activities measured

546 by using a dual-luciferase reporter assay system (Promega). All the luciferase activity values were
547 gained against the *Renilla* luciferase control. For each experiment, three independent experiments
548 were conducted, and each experiment was done in triplicate.
549
550 ***4.12 RNA binding protein immunoprecipitation (RIP)***
551 To identify whether MDA5 or MDA5-△RD can directly bind to SCRV viral RNA, MKC
552 cells (~$2.0 \times 10^7$) were transfected with pcDNA3.1-Flag, pcDNA3.1-MDA5-Flag or pcDNA3.1-
553 MDA5-△RD-Flag and then infected with SCRV at an MOI of 5 for 24 h. In addition, to identify
554 whether YTHDF1, YTHDF2, and YTHDF3 can directly bind to MDA5, MKC cells were co-
555 transfected with pcDNA3.1-Flag, pcDNA3.1-YTHDF1/2/3-Flag. For RNA immunoprecipitation
556 (RIP) assays, MKC cells were harvested after 48 h transfection, and RIP assays were carried out
557 with Magna RIP RNA-Binding Protein Immunoprecipitation Kit (Millipore) and anti-Flag
558 antibody (Abcam) following the manufacturer's protocol. Then, the expression of target gene
559 SCRV-M, SCRV-G, β-actin, or MDA5 were detected by quantitative real-time qRT-PCR analysis.
560
561 ***4.13 RNA Pull-Down assay***
562 Cytoplasmic extracts were prepared from $2 \times 10^7$ MKC cells transfected with mmiMDA5-Flag
563 (MDA5 of miiuy croaker) plasmids and $5 \times 10^7$ DF1 cells transfected with gga-MDA5-Flag
564 (MDA5 of chicken) plasmids. The extracts were incubated with biotinylated 5'ppp-RNA or
565 dsRNA and subjected to pull-down with streptavidin agarose beads (Geneseed), followed by
566 subsequent Coomassie bluestaining or SDS-PAGE analysis and immunoblotting with anti-Flag
567 antibody (Sigma).

568

569 ***4.14 EMSA assay***

570 Recombinant MDA5 proteins were mixed with biotin-labeled oligonucleotides in a reaction
571 mixture (10 μl: 20 mM Tris-HCl pH 8.0, 1.5 mM $MgCl_2$, 1.5 mM DTT). After incubation at room
572 temperature for 15 min, the reaction mixtures were conducted on 6% non-denaturing
573 polyacrylamide gels and the EMSA was performed using Chemiluminescent EMSA Kit
574 (Beyotime).

575

576 ***4.15 MeRIP-seq assays and analysis***

577 Total RNA was isolated using TRIzol reagent. $m^6A$ immunoprecipitation and library
578 preparation were performed following the manufacturer's protocol. Poly (A) RNA is purified from
579 50 μg total RNA using Dynabeads Oligo (dT) (Thermo Fisher) using two rounds of purification.
580 Then the poly(A) RNA was fragmented into small pieces using Magnesium RNA Fragmentation
581 Module (NEB) under 86°C for 7 min. Then the cleaved RNA fragments were incubated for 2 h at
582 4°C with $m^6A$-specific antibody (Synaptic Systems) in IP buffer (50 mM Tris-HCl, 750 mM NaCl
583 and 0.5% Igepal CA-630). Then the IP RNA was reverse-transcribed to create the cDNA by
584 SuperScript™ II Reverse Transcriptase (Invitrogen). The average insert size for the final cDNA
585 library was 300 ± 50 bp. For sequencing data analysis, we used HISAT2 to map reads to the
586 reference genome of *M. miiuy*. Mapped reads of IP and input libraries were provided for R
587 package exomePeak, which identifies $m^6A$ peaks with bed or bigwig format that can be adapted
588 for visualization on the IGV software. MEME and HOMER were used for de novo and known
589 motif finding followed by localization of the motif with respect to peak summit. Called peaks

590 were annotated by intersection with gene architecture using R package ChIPseeker. The
591 differentially expressed mRNAs were selected with log2 (fold change) >1 or log2 (fold change) <-
592 1 and *p*-value < 0.05 by R package edgeR. The circus map of $m^6A$ peaks in untreated and SCRV-
593 infected spleen tissues of *M. miiuy* was showed by TBtools[35].
594
595 ***4.16 MeRIP-qPCR***
596 Total RNA was extracted using TRIzol reagent (Invitrogen). Methylated $m^6A$ RNA
597 immunoprecipitation (Me-RIP) was performed according to the protocol of EpiQuik™
598 CUT&RUN $m^6A$ RNA Enrichment Kit (Epigentek). qPCR analysis of the methylated RNA was
599 performed to detect methylated MDA5 mRNA levels.
600
601 ***4.17 Total $m^6A$ Quantification Assay***
602 Total RNA was extracted by the TRIzol Reagent (Invitrogen). Then, an EpiQuik $m^6A$ RNA
603 Methylation Quantification Kit (EpiGentek) was used to detect the total $m^6A$ level according to
604 the manufacturer's protocol. Briefly, positive control (PC), negative control (NC), and 200 ng
605 isolated mRNA were added to each well with the capture antibody. Next, the RNA was incubated
606 with $m^6A$ antibody in wells, and $m^6A$ content was quantified at a wavelength of 450 nm.
607
608 ***4.18 RNA stability assays***
609 Cells were treated with actinomycin D (5 μg/mL) and then collected at different time points.
610 RNA was extracted by TRIzol reagent (Invitrogen), and the mRNA levels were measured using
611 qRT-PCR.

612

613 ***4.19 Database mining and sequence analysis***

614 The species tree is constructed by submitting species names to the NCBI
615 (https://www.ncbi.nlm.nih.gov/Taxonomy/CommonTree/wwwcmt.cgi). In order to determine
616 whether there is RIG-I in vertebrates, we use *H. sapiens* and *D. rerio* RIG-I protein sequences to
617 TBLASTN the whole genome sequence of the species on the ensemble website
618 (http://www.ensemble.org/). In addition, in order to prevent the possibility of incomplete species
619 genome, we also used RIG-I protein sequences of *H. sapiens* and *D. rerio* to compare the
620 transcriptome and genome sequenced of the designated species on NCBI website
621 (http://www.ncbi.nlm.nih.gov/Genbank/). For further gene synteny analysis, RIG-I of *H. sapiens*,
622 *C. milii, D. rerio* were used as anchor sites. In order to identify the MDA5 and LGP2 from *M.*
623 *miiuy*, we used the homologues of zebrafish reported previously as queries to seek for the
624 transcriptome[36] and a chromosome-scale genome database[37] of *M. miiuy* by using local
625 TBLASTN and BLASTN programs, then the protein structures were predicted by SMART
626 website (http://smart.embl-heidelberg.de/).

627

628 ***4.20 Statistical analysis***

629 Data are expressed as the mean ± SE from at least three independent triplicated
630 experiments. . A two-sided Student's t test was used to evaluate the data. The relative gene
631 expression data was acquired using the $2^{-\Delta\Delta CT}$ method, and comparisons between groups were
632 analyzed by one-way analysis of variance (ANOVA) followed by Duncan's multiple comparison
633 tests. A value of $p < 0.05$ was considered significant.

634

## Acknowledgements

This study was supported by the National Natural Science Foundation of China (31822057).

## Author contributions

S.G. designed and performed experiments, analyzed the data, performed bioinformatics analysis, and wrote the manuscript. X.L. performed experiments and provided advice in experimental plans. W.Z. provided advice in experimental plans. T.X. directed all the experiments and participated in experimental design, data analyses, interpretation, and manuscript writing.

## Declaration of interests

The authors declare no competing interests.

647 **References:**


648 1. Pichlmair, A. & Sousa, C. R. E. Innate recognition of viruses. *Immunity* **27**, 370-383 (2007).

649 2. Yoneyama, M., et al. Shared and unique functions of the DExD/H-box helicases RIG-I,
650 MDA5, and LGP2 in antiviral innate immunity. *Journal of Immunology* **175**, 2851-2858 (2005).

651 3. Kato, H., et al. Differential roles of MDA5 and RIG-I helicases in the recognition of RNA
652 viruses. *Nature* **441**, 101-105 (2006).

653 4. Hornung, V., et al. 5 '-triphosphate RNA is the ligand for RIG-I. *Science* **314**, 994-997
654 (2006).

655 5. Loo, Y.-M. & Gale, M., Jr. Immune Signaling by RIG-I-like Receptors. *Immunity* **34**, 680-
656 692 (2011).

657 6. Satoh, T., et al. LGP2 is a positive regulator of RIG-I- and MDA5-mediated antiviral
658 responses. *Proceedings of the National Academy of Sciences of the United States of America* **107**,
659 1512-1517 (2010).

660 7. Saito, T., et al. Regulation of innate antiviral defenses through a shared repressor domain in
661 RIG-I and LGP2. *Proceedings of the National Academy of Sciences of the United States of*
662 *America* **104**, 582-587 (2007).

663 8. Xu, L., et al. Loss of RIG-I leads to a functional replacement with MDA5 in the Chinese tree
664 shrew. *Proceedings of the National Academy of Sciences of the United States of America* **113**,
665 10950-10955 (2016).

666 9. Liang, B. & Su, J. Advances in aquatic animal RIG-I-like receptors. *Fish and shellfish*
667 *Immunology reports* **2**, 100012-100012 (2021).

668 10. Krchlikova, V., et al. Dynamic Evolution of Avian RNA Virus Sensors: Repeated Loss of

669 RIG-I and RIPLET. *Viruses-Basel* **15**, (2023).

670 11. Millet, J. K., Jaimes, J. A. & Whittaker, G. R. Molecular diversity of coronavirus host cell
671 entry receptors. *Fems Microbiology Reviews* **45**, (2021).

672 12. Walker, P. J., et al. ICTV Virus Taxonomy Profile: Rhabdoviridae 2022. *Journal of General*
673 *Virology* **103**, (2022).

674 13. Naz, S. S., Aslam, A. & Malik, T. An Overview of Immune Evasion Strategies of DNA and
675 RNA Viruses. *Infectious disorders drug targets* **21**, e300821192322 (2021).

676 14. Lou, X., Wang, J.-J., Wei, Y.-Q. & Sun, J.-J. Emerging role of RNA modification N6-
677 methyladenosine in immune evasion. *Cell Death & Disease* **12**, (2021).

678 15. Shi, H., Wei, J. & He, C. Where, When, and How: Context-Dependent Functions of RNA
679 Methylation Writers, Readers, and Erasers. *Molecular Cell* **74**, 640-650 (2019).

680 16. Zheng, G., et al. ALKBH5 Is a Mammalian RNA Demethylase that Impacts RNA
681 Metabolism and Mouse Fertility. *Molecular Cell* **49**, 18-29 (2013).

682 17. Jia, G., et al. N6-Methyladenosine in nuclear RNA is a major substrate of the obesity-
683 associated FTO. *Nature Chemical Biology* **7**, 885-887 (2011).

684 18. Wang, X., et al. N-6-methyladenosine-dependent regulation of messenger RNA stability.
685 *Nature* **505**, 117-+ (2014).

686 19. Zhang, Y., et al. RNA-binding protein YTHDF3 suppresses interferon-dependent antiviral
687 responses by promoting FOXO3 translation. *Proceedings of the National Academy of Sciences of*
688 *the United States of America* **116**, 976-981 (2019).

689 20. Lu, M., et al. N-6-methyladenosine modification enables viral RNA to escape recognition by
690 RNA sensor RIG-I. *Nature Microbiology* **5**, 584-+ (2020).

691 21. Wu, J., et al. N6-Methyladenosine Modification Opens a New Chapter in Circular RNA
692 Biology. *Frontiers in Cell and Developmental Biology* **9**, (2021).
693 22.
694 23. Chen, S. N., Zou, P. F. & Nie, P. Retinoic acid-inducible gene I (RIG-I)-like receptors (RLRs)
695 in fish: current knowledge and future perspectives. *Immunology* **151**, 16-25 (2017).
696 24. Zhou, Y., Zeng, P., Li, Y.-H., Zhang, Z. & Cui, Q. SRAMP: prediction of mammalian N-6-
697 methyladenosine (m(6)A) sites based on sequence-derived features. *Nucleic Acids Research* **44**,
698 (2016).
699 25. Xu, L., Yu, D., Fan, Y., Liu, Y.-P. & Yao, Y.-G. Evolutionary selection on MDA5 and LGP2 in
700 the chicken preserves antiviral competence in the absence of RIG-I. *Journal of Genetics and*
701 *Genomics* **46**, 499-503 (2019).
702 26. Schoggins, J. W., et al. A diverse range of gene products are effectors of the type I interferon
703 antiviral response (vol 472, pg 481, 2011). *Nature* **525**, (2015).
704 27. Wan, Q., Yang, C., Rao, Y., Liao, Z. & Su, J. MDA5 Induces a Stronger Interferon Response
705 than RIG-I to GCRV Infection through a Mechanism Involving the Phosphorylation and
706 Dimerization of IRF3 and IRF7 in CIK Cells. *Frontiers in Immunology* **8**, (2017).
707 28. Gan, L., Zhao, Y., Fu, Y. & Chen, Q. The potential role of m6A modifications on immune
708 cells and immunotherapy. *Biomedicine & Pharmacotherapy* **160**, (2023).
709 29. Durbin, A. F., Wang, C., Marcotrigiano, J. & Gehrke, L. RNAs Containing Modified
710 Nucleotides Fail To Trigger RIG-I Conformational Changes for Innate Immune Signaling. *Mbio* **7**,
711 (2016).
712 30. Rubio, R. M., Depledge, D. P., Bianco, C., Thompson, L. & Mohr, I. RNA m(6)A

713 modification enzymes shape innate responses to DNA by regulating interferon beta. *Genes &*
714 *Development* **32**, 1472-1484 (2018).
715 31. Winkler, R., et al. m(6)A modification controls the innate immune response to infection by
716 targeting type I interferons. *Nature Immunology* **20**, 173-+ (2019).
717 32. Geng, S., et al. The m6A Reader YTHDF2 Modulates Antiviral and Antibacterial Activity by
718 Suppressing METTL3 Methylation-Modified STING in Fish. *Journal of immunology (Baltimore,*
719 *Md. : 1950)* **210**, 653-667 (2023).
720 33. Chu, Q., Xu, T., Zheng, W., Chang, R. & Zhang, L. Long noncoding RNA MARL regulates
721 antiviral responses through suppression miR-122-dependent MAVS downregulation in lower
722 vertebrates. *Plos Pathogens* **16**, (2020).
723 34. Geng, S., Zheng, W., Zhao, Y. & Xu, T. FTO promotes innate immunity by controlling NOD1
724 expression via m6A-YTHDF2 manner in teleost. *Iscience* **25**, (2022).
725 35. Chen, C., et al. TBtools: An Integrative Toolkit Developed for Interactive Analyses of Big
726 Biological Data. *Molecular Plant* **13**, 1194-1202 (2020).
727 36. Che, R. B., Sun, Y. Y., Sun, D. Q. & Xu, T. J. Characterization of the Miiuy Croaker
728 (Miichthys miiuy) Transcriptome and Development of Immune-Relevant Genes and Molecular
729 Markers. *Plos One* **9**, (2014).
730 37. Xu, T., Li, Y., Zheng, W., & Sun, Y. A chromosome-level genome assembly of the miiuy
731 croaker (*Miichthys miiuy*) using nanopore sequencing and Hi-C. *Aquaculture and Fisheries*.
732 10.1016/j.aaf.2021.06.001 (2021).
733

734 **Figure Legends:**

735 **Figure 1. A genetic compensation response model for RIG loss.** (A) Loss of RIG-I in
736 vertebrates. Each branch tip represents one species. Red lines show lineages where loss of RIG-I.
737 The red circle indicates the occurrence of an independent loss event. Branch lengths scale in
738 millions of years (MYA). (B) Comparative analysis of gene synteny of RIG-I in vertebrate
739 genomes. (C and D) SCRV-RNA and VSV-RNA were extracted from SCRV and VSV virus and
740 dephosphorylated them with Calf Intestinal Alkaline Phosphatase (CIAP). Then, MKC cells were
741 transfected with SCRV-RNA and SCRV-RNA+CIAP, and DF-1 cells were transfected with VSV-
742 RNA and VSV-RNA+CIAP. IRF3 dimerization was analyzed by native gel electrophoresis. (E)
743 MKC cells were transfected with different concentrations of SCRV-RNA and SCRV-RNA+CIAP,
744 then the expression of IFN-1 was detected by qRT-PCR. (F) Predicted protein structures of MDA5
745 and LGP2 of *M. miiuy* and RIG-I of *H. sapiens*. (G) The expression of MDA5 and LGP2 plasmids
746 of *M. miiuy* were detected by Western Blot. (H and I) MKC cells were co-transfected with MDA5
747 plasmids and LGP2 plasmids (H) or si-LGP2 (I) for 24 h and then treated with SCRV (MOI = 5)
748 for 24 h. The expression of IFN-1 was determined by qPCR. (J) A genetic compensation response
749 model for RIG loss. All data presented as the means ± SE from at least three independent
750 triplicated experiments. **, $p < 0.01$ versus the controls.

751

752 **Figure 2. MDA5 promotes host antiviral innate immunity.** (A) Silence efficiency of si-MDA5
753 measured by qRT-PCR and Western blotting. Two siRNAs of MDA5 were transfected into MPC
754 cells for 48 h respectively. (B) MKC cells were transfected with MDA5 plasmids for 48 h, then
755 the overexpression efficiency was detected through MDA5 endogenous antibodies. (C)

756 Subcellular localization of MDA5 in MKCs by immunofluorescence. (D) MDA5 knockdown
757 suppresses NF-κB, IRF3, IRF7, and IFN-1 signaling. MPC cells were transfected with pRL-TK
758 Renilla luciferase plasmid, luciferase reporter genes, together with MDA5 expression plasmid. At
759 48 h post-transaction, the luciferase activity was measured and normalized to renilla luciferase
760 activity. (E) Knockdown of MDA5 attenuates the expression of antiviral genes. MPC cells were
761 transfected with si-Ctrl or si-MDA5 for 24 h and then treated with SCRV (MOI =5) or poly(I:C)-
762 HMW for 24 h. The expression of IFN-1, Mx1, ISG15, and Viperin were determined by qPCR. (F
763 and G) Overexpression of MDA5 promotes the expression of antiviral genes. MKC cells were
764 transfected with vector or MDA5 expression plasmids for 24 h and then treated with SCRV (MOI
765 = 5) or poly (I:C)-HMW for 24 h. The expression of MDA5 (F), and antiviral genes, including
766 IFN-1, Mx1, ISG15, and Viperin (G) were determined by qPCR. (H and J) MPC cells transfected
767 with si-Ctrl or si-MDA5 and MKC cells transfected with pcDNA3.1 vector or MDA5 plasmid 24
768 h and then treated with SCRV at the dose indicated for 48 h. Then, cell monolayers were fixed
769 with 4% paraformaldehyde and stained with 1% crystal violet. (I and K) MDA5 inhibits SCRV
770 replication. MPC cells were transfected with si-Ctrl or si-MDA5 and MKC cells were transfected
771 with pcDNA3.1 vector or MDA5 expression plasmid for 24 h, then infected with SCRV (MOI =
772 5) for 12, 24, or 48 h. The qPCR analysis was conducted for SCRV-M and SCRV-G RNA levels.
773 (L and M) MDA5 immunoprecipitates with MAVS (L) and STING (M). EPC cells (~ $1\times10^7$) were
774 co-transfected with MAVS-Myc or STING-Myc and MDA5-Flag expression plasmids for 24 h,
775 followed by immunoprecipitation (IP) with anti-Myc. (N and O) MKC cells were transfected with
776 MDA5 plasmids and STING plasmids (N) or si-STING (O) for 24 h and then treated with SCRV
777 (MOI = 5) for 24 h. The expression of IFN-1 was determined by qPCR. (P and Q) MKC cells were

778 transfected with MDA5 plasmids and si-STING for 24 h and then transfected with SCRV-RNA for
779 24 h, then the IRF3 dimerization and IFN-1 levels were analyzed by native gel electrophoresis (P)
780 and qPCR (Q), respectively. All data presented as the means ± SE from at least three independent
781 triplicated experiments. **, $p < 0.01$; *, $p < 0.05$ versus the controls.
782
783 **Figure 3. RD domain is required for MDA5 to recognize SCRV RNA.** (A) The association of
784 MDA5 proteins with SCRV. (B) Schematics and expression of MDA5 and truncated MDA5
785 (MDA5-△RD). (C) The association of MDA5 and MDA5-△RD proteins with SCRV. (D) MKC
786 cells transfected with pcDNA3.1 vector, MDA5, or MDA5-△RD plasmids for 24 h and then
787 treated with SCRV at the dose indicated for 48 h. Then, cell monolayers were fixed with 4%
788 paraformaldehyde and stained with 1% crystal violet. (E) MKC cells were transfected with
789 pcDNA3.1 vector, MDA5 or MDA5-△RD expression plasmids for 24 h, then infected with SCRV
790 for 24 h, then the qPCR analysis was conducted for SCRV-M and SCRV-G RNA levels. (F and G)
791 Expression antiviral genes in poly(I:C)-HMW-stimulated (F) or SCRV-infected (G) MKC cells
792 transfected with pcDNA3.1 vector, MDA5, or MDA5-△RD expression plasmids. All data
793 presented as the means ± SE from at least three independent triplicated experiments. **, $p < 0.01$;
794 *, $p < 0.05$ versus the controls.
795
796 **Figure 4. MDA5 recognizes 5'ppp-RNA in *M. miiuy and G. gallus*.** (A) Schematic
797 representation of 5'ppp-SCRV and dsRNA. The product of in vitro transcription runs as a single
798 product degraded by RNase I. (B) Pull-down of biotinylated or non-biotinylated dsRNA and
799 5'ppp-SCRV by mmiMDA5. MKC cells were transfected with mmiMDA5-Flag plasmid, and the

800 input and immunoprecipitated MDA5 proteins were analyzed by Western blot. (C) MKC cells
801 were transfected with 5'ppp-SCRV, 5'OH-SCRV (5'ppp-SCRV dephosphorylated by CIAP), or
802 5'pppGG-SCRV (5'ppp-SCRV capped by m7G cap analog), then IRF3 dimerization was analyzed
803 by native gel electrophoresis. (D) The cytoplasmic fraction of MKC cells transfected with Flag-
804 tagged mmiMDA5 was incubated with biotinylated 5'ppp-SCRV, 5'OH-SCRV, or 5'pppGG-
805 SCRV. RNA-protein complexes were pulled down using streptavidin affinity beads. Input and
806 pull-down samples were analyzed by SDS-PAGE and immunoblotting using anti-Flag antibody.
807 (E) Purity of recombinant mmiMDA5 and mmiMDA5-△RD were determined by SDS-PAGE and
808 immunoblotting using anti-His antibody. (F) EMSA of 5'ppp-SCRV with mmiMDA5. For binding
809 competition, indicated non-biotinylated RNAs (50-fold molar excess over the probe) were
810 included. (G) EMSA of 5'ppp-SCRV with mmiMDA5 or mmiMDA5-△RD. (H) Schematic
811 representation of 5'ppp-VSV. The product of in vitro transcription runs as a single product
812 degraded by RNase I. (I) Pull-down of dsRNA and 5'ppp-VSV by ggaMDA5. DF-1 cells were
813 transfected with ggaMDA5-Flag plasmids, and the input and immunoprecipitated MDA5 proteins
814 were analyzed by Western blot. (J) DF-1 cells were transfected with 5'ppp-VSV, 5'OH-VSV
815 (5'ppp-VSV dephosphorylated by CIAP), or 5'pppGG-VSV (5'ppp-VSV capped by m7G cap
816 analog), then IRF3 dimerization was analyzed by native gel electrophoresis. (K)The cytoplasmic
817 fraction of DF-1 cells transfected with Flag-tagged ggaMDA5 was incubated with biotinylated
818 5'ppp-VSA, 5'OH-VSV, or 5'pppGG-RNA. RNA-protein complexes were pulled down using
819 streptavidin affinity beads. Input and pull-down samples were analyzed by SDS-PAGE and
820 immunoblotting using anti-Flag antibody. (L) EMSA of 5'ppp-RNA with ggaMDA5. For binding
821 competition, indicated non-biotinylated RNAs (50-fold molar excess over the probe) were

822 included.

823

824 **Figure 5. Increased m$^6$A modification and expression of MDA5 upon SCRV infection.** (A)
825 Schematic of the MeRIP-seq protocol used to identify differential m$^6$A methylation following
826 infection of *M. miiuy* spleen tissues with SCRV. (B) Circos plots showing differentially m$^6$A-
827 methylated peaks identified from normal and SCRV-infected spleen tissues of *M. miiuy*. The green
828 and red lines on the innermost ring represented the m$^6$A peaks identified from normal and SCRV-
829 infected spleen tissues of *M. miiuy* respectively. The orange lines represent the log2 fold change
830 values for each differentially m$^6$A peak. The blue spots represent the fold change of gene
831 expression. Chromosomes were shown on the outermost ring, the ruler on which represented the
832 physical distance is in millions of bases (Mb). (C) The m$^6$A abundance in MDA5 mRNA
833 transcripts detected by MeRIP-seq, the m$^6$A peak of MDA5 is circled in the green box. (D) The
834 exon1 sequence of MDA5 was submitted to the SRAMP website, and then the predicted m$^6$A site
835 was displayed. Four predicted methylation sites located on the exon1 of MDA5 were marked by
836 red box, then we designed two m$^6$A specific primers (MDA5-m$^6$A-1 and MDA5-m$^6$A-2). (E) m$^6$A
837 abundance on MDA5 exon1 detected by MeRIP-qPCR and emiquantitative PCR in MKC cells.
838 (F) MeRIP-qPCR analysis of relative m$^6$A level of MDA5 in Mock, SCRV-infected, and
839 poly(I:C)-HMW-stimulated MKC cells. (G) mRNA levels of MDA5 in spleen and kidney tissues
840 measured by qRT-PCR at indicated time after SCRV infection (MOI = 5). (H and I) mRNA and
841 protein levels of MDA5 in MKC cells measured by qRT-PCR and Western blotting at indicated
842 time after SCRV infection (MOI = 5) (H) and poly(I:C)-HMW stimulation (I). All data presented
843 as the means ± SE from at least three independent triplicated experiments. **, $p < 0.01$ versus the

844 controls.

845

846 **Figure 6. m$^6$A-modification weakens MDA5 mRNA stability and antiviral ability.** (A) Silence
847 efficiency of si-METTL3 and si-METTL14 measured. Three siRNAs of METTL3 and METTL14
848 were transfected into MPC cells for 48 h respectively. (B) METTL3 immunoprecipitates with
849 METTL14. EPC cells ($1\times10^7$) were co-transfected with METTL3-Myc and METTL14-Flag
850 expression plasmids for 24 h, followed by immunoprecipitation (IP) with anti-Myc. (C) METTL3
851 and METTL14 significantly increased the m$^6$A content. MPCs were transfected with si-Ctrl or si-
852 METTL3 or si-METTL14 and MKCs were transfected with vector or METTL3 or METTL14
853 plasmids for 48 h, then the m$^6$A level was measured by colorimetry. (D) METTL3 and METTL14
854 overexpressed MKC cells seeded in 48-well plates overnight were treated with SCRV at the dose
855 indicated for 48 h. Then, cell monolayers were fixed with 4% paraformaldehyde and stained with
856 1% crystal violet. (E) MKC cells were transfected with pcDNA3.1 vector and METTL3 or
857 METTL14 expression plasmid for 24 h, then infected with SCRV (MOI = 5) for 24 h. The qPCR
858 analysis was conducted for SCRV-M and SCRV-G RNA levels. (F) The m$^6$A level alteration of
859 MDA5 upon METTL3 or METTL14 knockdown or overexpression was examined by MeRIP-
860 qPCR. MPC cells were transfected with si-Ctrl or si-METT3 and MKC cells were transfected with
861 vector or METTL3 or METTL14 plasmids for 48 h. (G and H) MPC cells were transfected with
862 si-Ctrl, si-METTL3 or METTL14 and MKC cells were transfected with vector, METTL3, or
863 METTL14 plasmids for 48 h, the expression of MDA5 was detected by qRT-PCR and Western
864 blotting. (I) MPC cells were transfected with si-Ctrl, si-METTL3, or si-METTL14, and MKC cells
865 were transfected with vector, METTL3, or METTL14 plasmids, then 5 μg/ml actinomycin D was

added to the cells for 0 h, 2 h, and 4 h. The half-life of MDA5 was analyzed by qRT-PCR. (J) MKC cells were transfected with vector or METTL3&14 plasmids for 24 h and then treated with Cycloleucine (CL) for 24 h in a final concentration of 20 mM. The expression of MDA5 was detected by qRT-PCR and Western blotting. (K) MKC cells were transfected with vector or METTL3&14 plasmids for 24 h and then treated with CL for 24 h at 20 mM, then 5 μg/ml actinomycin D was added to the cells for 0 h, 2 h, and 4 h. The half-life of MDA5 was analyzed by qRT-PCR. (L) MKC cells were transfected with vector or METTL3&14 plasmids for 24 h and stimulated with SCRV (MOI = 5) for 24 h, then the expression of MDA5 was detected by qRT-PCR and Western blotting. (M) MKC cells seeded in 48-well plates overnight were transfected with MDA5 or MDA5+METTL3&14 plasmids for 48 h, then the expression of MDA5 was detected by qRT-PCR. (N) MKC cells seeded in 48-well plates overnight were transfected with MDA5 or MDA5+METTL3&14 plasmids were treated with SCRV at the dose indicated for 48 h. Then, cell monolayers were fixed with 4% paraformaldehyde and stained with 1% crystal violet. (O) MKC cells were transfected with MDA5 or MDA5 + METTL3&14 plasmids for 24 h, then infected with SCRV (MOI = 5) for 24 h. The qPCR analysis was conducted for SCRV-M and SCRV-G RNA levels. All data presented as the means ± SE from at least three independent triplicated experiments. **, $p < 0.01$; *, $p < 0.05$ versus the controls.

**Figure 7. Detailed m$^6$A regulatory mechanism of MDA5.** (A) The binding relationship between YTHDF1, YTHDF2, or YTHDF3 and MDA5 mRNA was validated using a RIP assay. MKC cells were transfected with YTHDF1-Flag, YTHDF2-Flag, YTHDF3-Flag, or pcDNA3.1-Flag for 48 h. (B) SiRNA silencing effect test of YTHDF1, YTHDF2, and YTHDF3. MPC cells were transfected

888 with si-YTHDF1, si-YTHDF2, or si-YTHDF3 for 48 h. (C and D) MPC cells were transfected
889 with si-YTHDF1, si-YTHDF2, si-YTHDF3 or si-Ctrl (C), and MKC cells were transfected with
890 YTHDF1, YTHDF2, YTHDF3 or vector for 48 h (D), then the expression of MDA5 was detected
891 by qRT-PCR and Western blotting. (E) Relative mRNA and protein levels of MDA5 in MKC cells
892 after co-transfected with YTHDF2&3 plasmids and si-METTL3&14 by qPCR and western blot
893 assays. (F) MKC cells were transfected with YTHDF2&3 plasmids and si-METTL3&14, then 5
894 μg/ml actinomycin D was added to the cells for 0 h, 2 h, and 4 h. The half-life of MDA5 was
895 analyzed by qRT-PCR. (G) MKC cells were transfected with vector, FTO, ALKBH5 plasmids for
896 48 h, then the expression of MDA5 was detected by qRT-PCR and Western blotting. (H) Relative
897 mRNA and protein levels of MDA5 in MKC cells after co-transfected with YTHDF2&3 plasmids
898 and FTO plasmids by qPCR and western blotting. (I) MKC cells were transfected with
899 YTHDF2&3 plasmids and FTO plasmids, then 5 μg/ml actinomycin D was added to the cells for 0
900 h, 2 h, and 4 h. The half-life of MDA5 was analyzed by qRT-PCR. (J) Schematic diagram of arms
901 race between MDA5 and 5'ppp-RNA virus in *M. miiuy*.
902

903 **Supporting Information**

904 **Supplementary file 1.** PCR primer information in this study.
905

906 **Figure 6-figure supplement 1. The regulation of m$^6$A writers (METTL3&14) to the MDA5-**
907 **exon1.** (A) Relative luciferase activity of pmirGLO-MDA5-exon1 firefly luciferase reporters in
908 MPC cells transfected with si-Ctrl, si-METTL3 or si-METTL14. (B) Schematic diagram of m$^6$A
909 site mutation on exon1 of MDA5. 'A' in the predicted methylation motif was replaced by 'U'. (C)

910 Relative luciferase activity of wild-type or mutant pmirGLO-MDA5-exon1 firefly luciferase
911 reporter in MPC cells transfected with si-Ctrl or si-METTL3&14. (D) METTL3 and METTL14
912 could downregulate GFP expression of mVenus-MDA5-exon1. EPC cells were co-transfected with
913 the mVenus-MDA5-exon1 and vector, METTL3 or METTL14 plasmids. At 48 h post-transfection,
914 the fluorescence intensity and the GFP expression were evaluated by enzyme-labeled instrument
915 and western blotting, respectively. All data presented as the means ± SE from at least three
916 independent triplicated experiments. **, $p < 0.01$ versus the controls.
917
918 **Figure 7-figure supplement 1. The regulation of YTHDF readers (YTHDF1&2&3) to the**
919 **MDA5-exon1.** (A) Relative luciferase activity of pmirGLO-MDA5-exon1 firefly luciferase
920 reporters in MPC cells transfected with si-Ctrl, si-YTHDF1, si-YTHDF2 or si-YTHDF3. (B)
921 Relative luciferase activity of wild-type or mutant pmirGLO-MDA5-exon1 plasmids in MPC cells
922 transfected with si-Ctrl or si-YTHDF2&3. (C) YTHDF2 and YTHDF3 could downregulate GFP
923 expression of mVenus-MDA5-exon1. EPC cells were co-transfected with the mVenus-MDA5-
924 exon1 and vector, YTHDF1, YTHDF2 or YTHDF3 plasmids. At 48 h post-transfection, the
925 fluorescence intensity and the GFP expression were evaluated by enzyme-labeled instrument and
926 western blotting, respectively. All data presented as the means ± SE from at least three
927 independent triplicated experiments. **, $p < 0.01$ versus the controls.
928

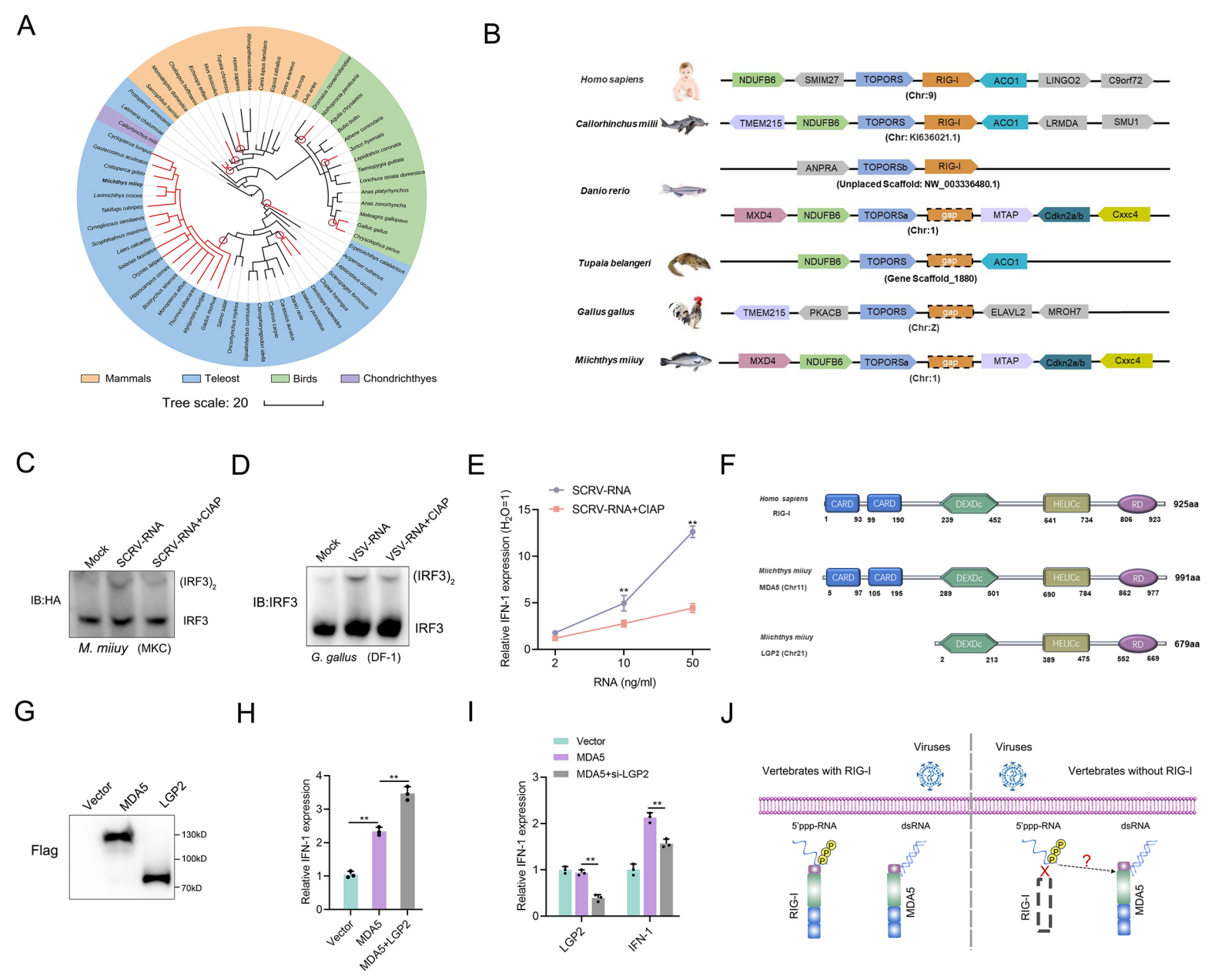
A
Mammals
Teleost
Birds
Chondrichthyes
Tree scale: 20
B
Homo sapiens
NDUFB6
SMIM27
TOPORS
RIG-I
ACO1
LINGO2
C9orf72
(Chr:9)
Callorhinchus milii
TMEM215
NDUFB6
TOPORS
RIG-I
ACO1
LRMDA
SMU1
(Chr: KI636021.1)
Danio rerio
ANPRA
TOPORSb
RIG-I
(Unplaced Scaffold: NW_003336480.1)
MXD4
NDUFB6
TOPORSa
gap
MTAP
Cdkn2a/b
Cxxc4
(Chr:1)
Tupaia belangeri
NDUFB6
TOPORS
gap
ACO1
(Gene Scaffold_1880)
Gallus gallus
TMEM215
PKACB
TOPORS
gap
ELAVL2
MROH7
(Chr:Z)
Miichthys miiuy
MXD4
NDUFB6
TOPORSa
gap
MTAP
Cdkn2a/b
Cxxc4
(Chr:1)
C
Mock
SCRV-RNA
SCRV-RNA+CIAP
IB:HA
(IRF3)2
IRF3
M. miiuy (MKC)
D
Mock
VSV-RNA
VSV-RNA+CIAP
IB:IRF3
(IRF3)2
IRF3
G. gallus (DF-1)
E
SCRV-RNA
SCRV-RNA+CIAP
Relative IFN-1 expression (H2O=1)
RNA (ng/ml)
F
Homo sapiens
RIG-I
CARD
CARD
DEXDc
HELICc
RD
925aa
Miichthys miiuy
MDA5 (Chr11)
991aa
Miichthys miiuy
LGP2 (Chr21)
679aa
G
Vector
MDA5
LGP2
Flag
130kD
100kD
70kD
H
Relative IFN-1 expression
Vector
MDA5
MDA5+LGP2
I
Vector
MDA5
MDA5+si-LGP2
Relative IFN-1 expression
LGP2
IFN-1
J
Viruses
Viruses
Vertebrates with RIG-I
Vertebrates without RIG-I
5'ppp-RNA
dsRNA
5'ppp-RNA
dsRNA
RIG-I
MDA5
RIG-I
MDA5

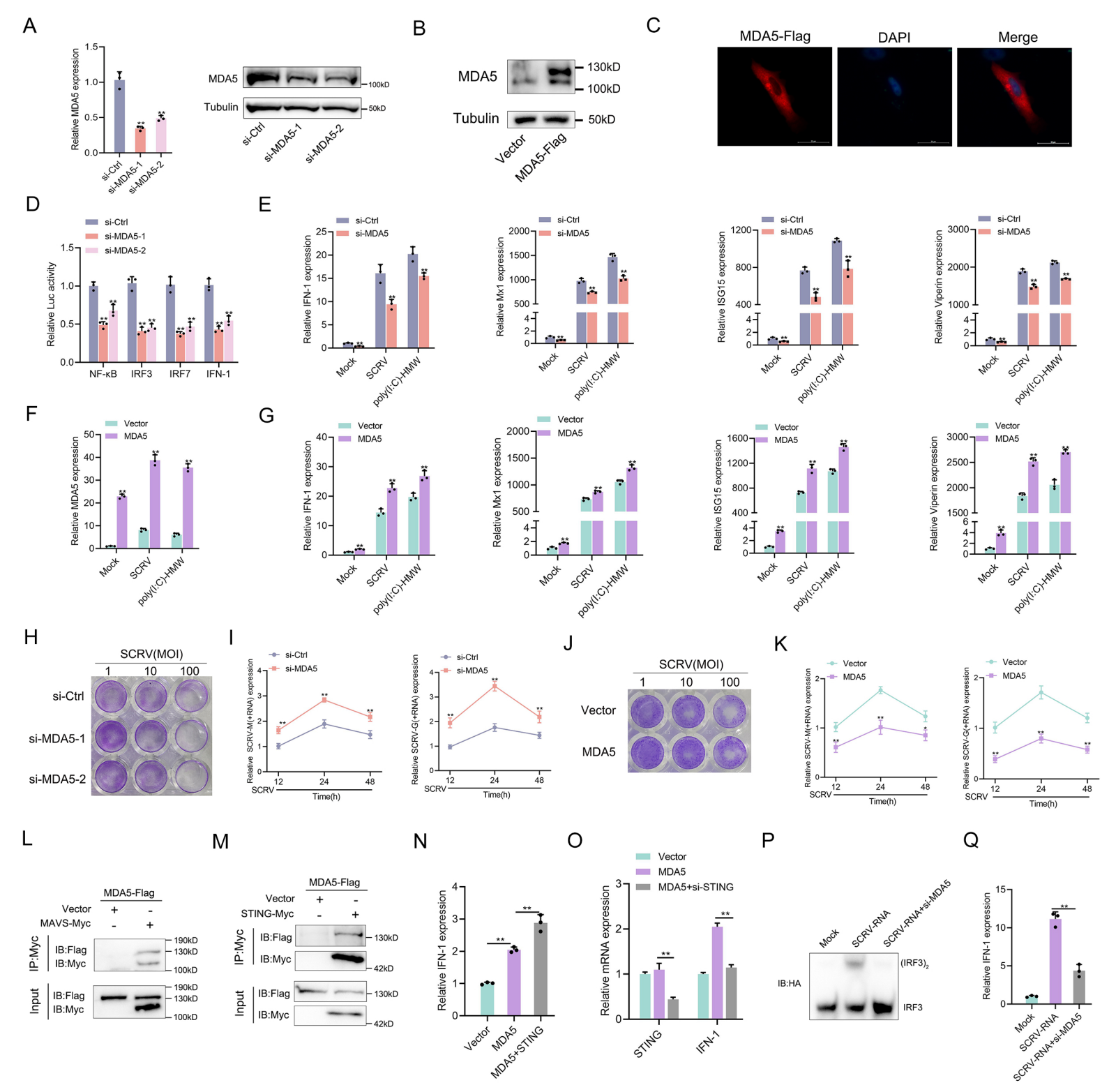
A
Relative MDA5 expression
si-Ctrl
si-MDA5-1
si-MDA5-2
MDA5
Tubulin
100kD
50kD
B
MDA5
Tubulin
130kD
100kD
50kD
Vector
MDA5-Flag
C
MDA5-Flag
DAPI
Merge
D
Relative Luc activity
NF-κB
IRF3
IRF7
IFN-1
E
Relative IFN-1 expression
Relative Mx1 expression
Relative ISG15 expression
Relative Viperin expression
Mock
SCRV
poly(I:C)-HMW
F
Relative MDA5 expression
G
H
SCRV(MOI)
1
10
100
I
Relative SCRV-M(+RNA) expression
Relative SCRV-G(+RNA) expression
Time(h)
J
K
L
MDA5-Flag
MAVS-Myc
IP:Myc
Input
IB:Flag
IB:Myc
190kD
130kD
100kD
M
STING-Myc
42kD
N
Relative IFN-1 expression
MDA5+STING
O
Relative mRNA expression
STING
IFN-1
P
SCRV-RNA
SCRV-RNA+si-MDA5
IB:HA
(IRF3)2
IRF3
Q

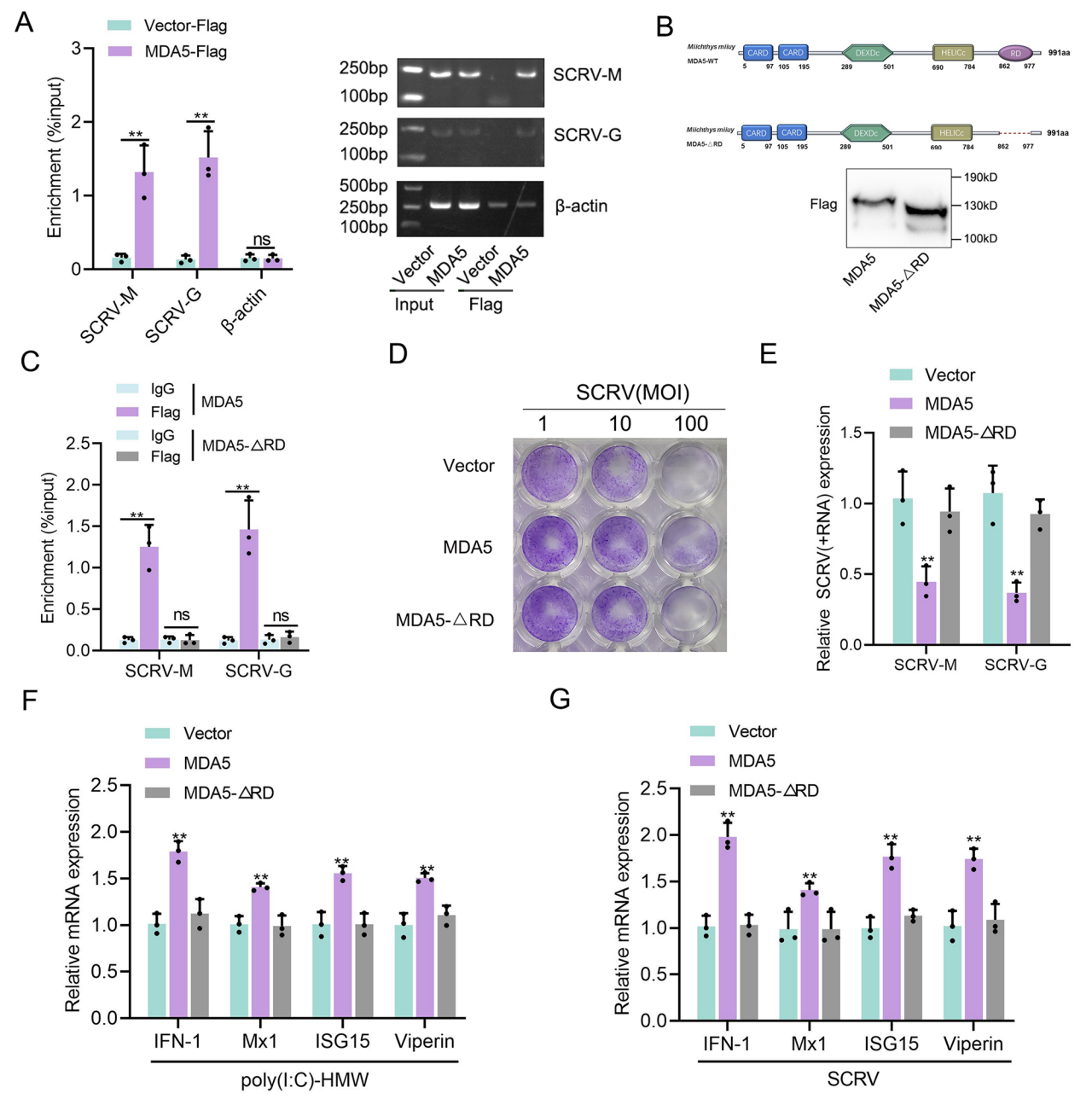
A
Vector-Flag
MDA5-Flag
Enrichment (%input)
SCRV-M
SCRV-G
β-actin
ns
250bp
100bp
500bp
Vector
MDA5
Input
Flag
B
Miichthys miluy
MDA5-WT
CARD
DEXDc
HELICc
RD
991aa
MDA5-△RD
Flag
190kD
130kD
100kD
C
IgG
Flag
MDA5
MDA5-△RD
D
SCRV(MOI)
1
10
100
Vector
MDA5
MDA5-△RD
E
Relative SCRV(+RNA) expression
F
Relative mRNA expression
IFN-1
Mx1
ISG15
Viperin
poly(I:C)-HMW
G
SCRV

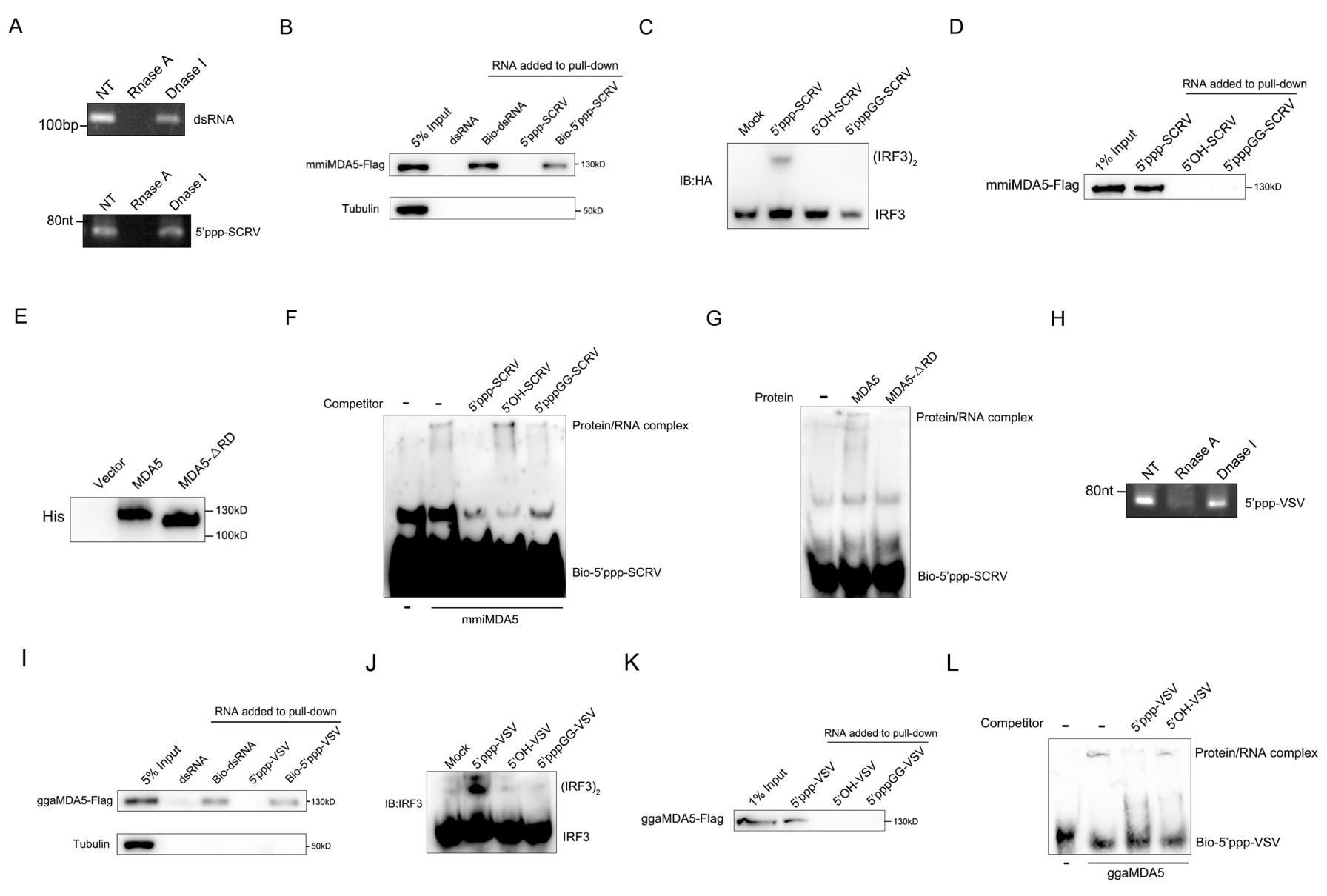
A
NT
Rnase A
Dnase I
100bp
dsRNA
80nt
5'ppp-SCRV
B
RNA added to pull-down
5% Input
dsRNA
Bio-dsRNA
5'ppp-SCRV
Bio-5'ppp-SCRV
mmiMDA5-Flag
130kD
Tubulin
50kD
C
Mock
5'ppp-SCRV
5'OH-SCRV
5'pppGG-SCRV
IB:HA
(IRF3)2
IRF3
D
RNA added to pull-down
1% Input
5'ppp-SCRV
5'OH-SCRV
5'pppGG-SCRV
mmiMDA5-Flag
130kD
E
Vector
MDA5
MDA5-△RD
His
130kD
100kD
F
Competitor
5'ppp-SCRV
5'OH-SCRV
5'pppGG-SCRV
Protein/RNA complex
Bio-5'ppp-SCRV
mmiMDA5
G
Protein
MDA5
MDA5-△RD
Protein/RNA complex
Bio-5'ppp-SCRV
H
NT
Rnase A
Dnase I
80nt
5'ppp-VSV
I
RNA added to pull-down
5% Input
dsRNA
Bio-dsRNA
5'ppp-VSV
Bio-5'ppp-VSV
ggaMDA5-Flag
130kD
Tubulin
50kD
J
Mock
5'ppp-VSV
5'OH-VSV
5'pppGG-VSV
IB:IRF3
(IRF3)2
IRF3
K
RNA added to pull-down
1% Input
5'ppp-VSV
5'OH-VSV
5'pppGG-VSV
ggaMDA5-Flag
130kD
L
Competitor
5'ppp-VSV
5'OH-VSV
Protein/RNA complex
Bio-5'ppp-VSV
ggaMDA5

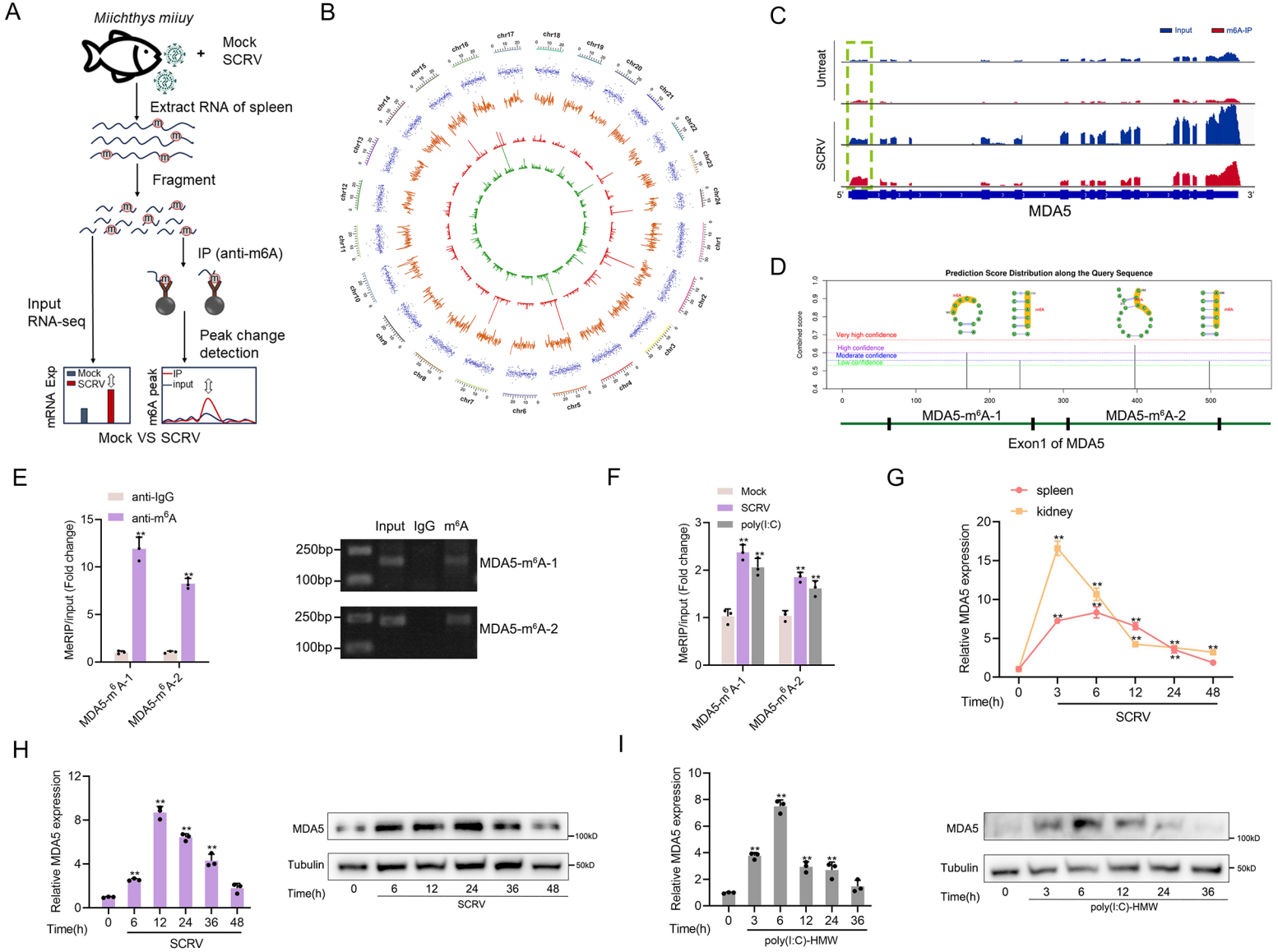
A
Miichthys miiuy
Mock
SCRV
Extract RNA of spleen
Fragment
IP (anti-m6A)
Input
RNA-seq
Peak change
detection
mRNA Exp
Mock
SCRV
m6A peak
IP
input
Mock VS SCRV
B
C
Input
m6A-IP
Untreat
SCRV
5'
3'
MDA5
D
Prediction Score Distribution along the Query Sequence
Combined score
Very high confidence
High confidence
Moderate confidence
Low confidence
MDA5-m6A-1
MDA5-m6A-2
Exon1 of MDA5
E
anti-IgG
anti-m6A
MeRIP/input (Fold change)
MDA5-m6A-1
MDA5-m6A-2
Input
IgG
m6A
250bp
100bp
F
Mock
SCRV
poly(I:C)
MeRIP/input (Fold change)
G
spleen
kidney
Relative MDA5 expression
Time(h)
SCRV
H
Relative MDA5 expression
Time(h)
SCRV
MDA5
Tubulin
100kD
50kD
I
Relative MDA5 expression
Time(h)
poly(I:C)-HMW

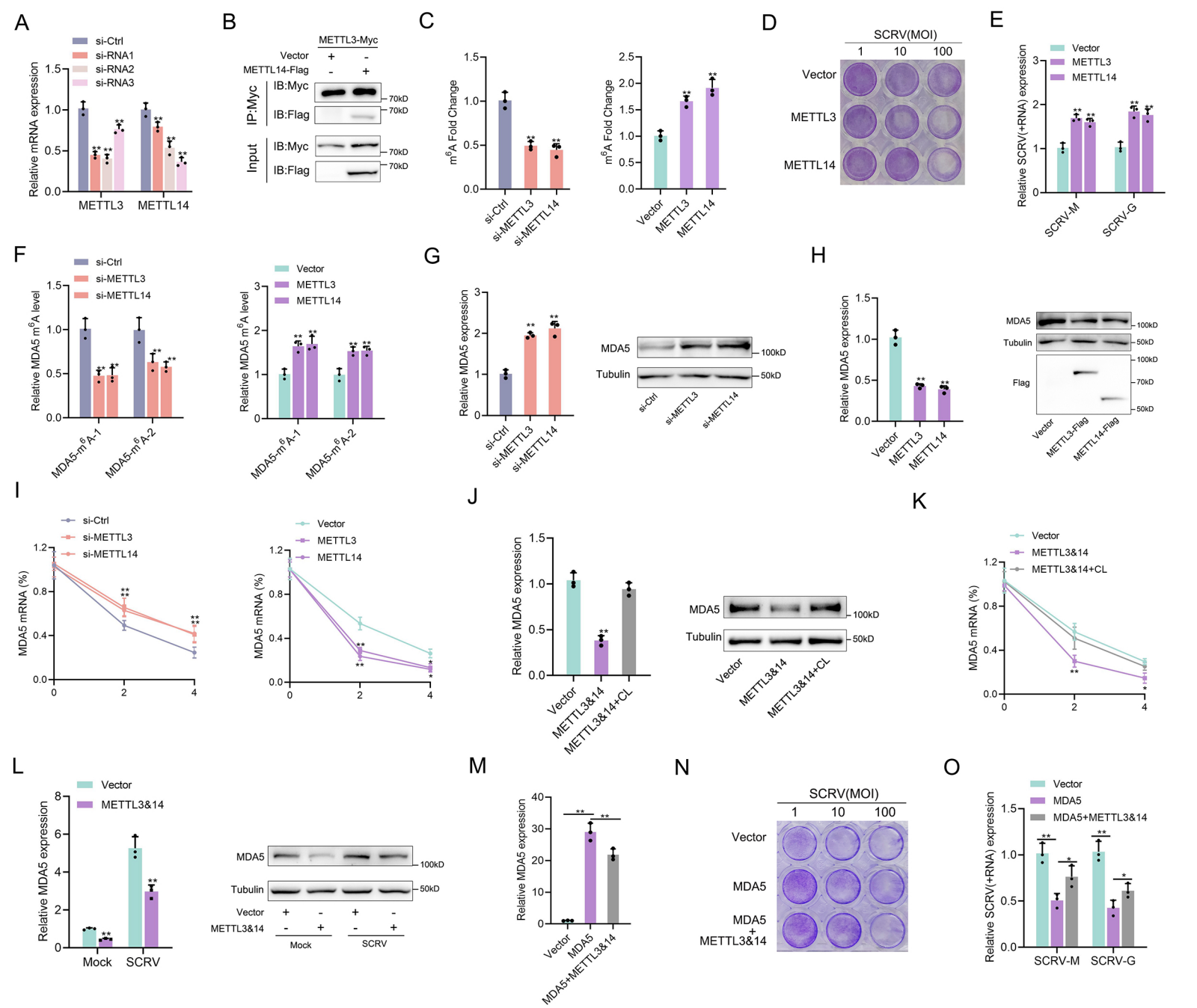
A
si-Ctrl
si-RNA1
si-RNA2
si-RNA3
Relative mRNA expression
METTL3
METTL14
B
METTL3-Myc
Vector
METTL14-Flag
IP:Myc
IB:Myc
IB:Flag
Input
IB:Myc
IB:Flag
70kD
C
m6A Fold Change
si-Ctrl
si-METTL3
si-METTL14
Vector
METTL3
METTL14
D
SCRV(MOI)
1
10
100
Vector
METTL3
METTL14
E
Vector
METTL3
METTL14
Relative SCRV(+RNA) expression
SCRV-M
SCRV-G
F
si-Ctrl
si-METTL3
si-METTL14
Relative MDA5 m6A level
MDA5-m6A-1
MDA5-m6A-2
Vector
METTL3
METTL14
G
Relative MDA5 expression
si-Ctrl
si-METTL3
si-METTL14
MDA5
Tubulin
100kD
50kD
H
Relative MDA5 expression
Vector
METTL3
METTL14
MDA5
Tubulin
Flag
100kD
70kD
50kD
Vector
METTL3-Flag
METTL14-Flag
I
si-Ctrl
si-METTL3
si-METTL14
MDA5 mRNA (%)
Vector
METTL3
METTL14
J
Relative MDA5 expression
Vector
METTL3&14
METTL3&14+CL
MDA5
Tubulin
100kD
50kD
K
Vector
METTL3&14
METTL3&14+CL
MDA5 mRNA (%)
L
Vector
METTL3&14
Relative MDA5 expression
Mock
SCRV
MDA5
Tubulin
100kD
50kD
Vector
METTL3&14
Mock
SCRV
M
Relative MDA5 expression
Vector
MDA5
MDA5+METTL3&14
N
SCRV(MOI)
1
10
100
Vector
MDA5
MDA5 + METTL3&14
O
Vector
MDA5
MDA5+METTL3&14
Relative SCRV(+RNA) expression
SCRV-M
SCRV-G

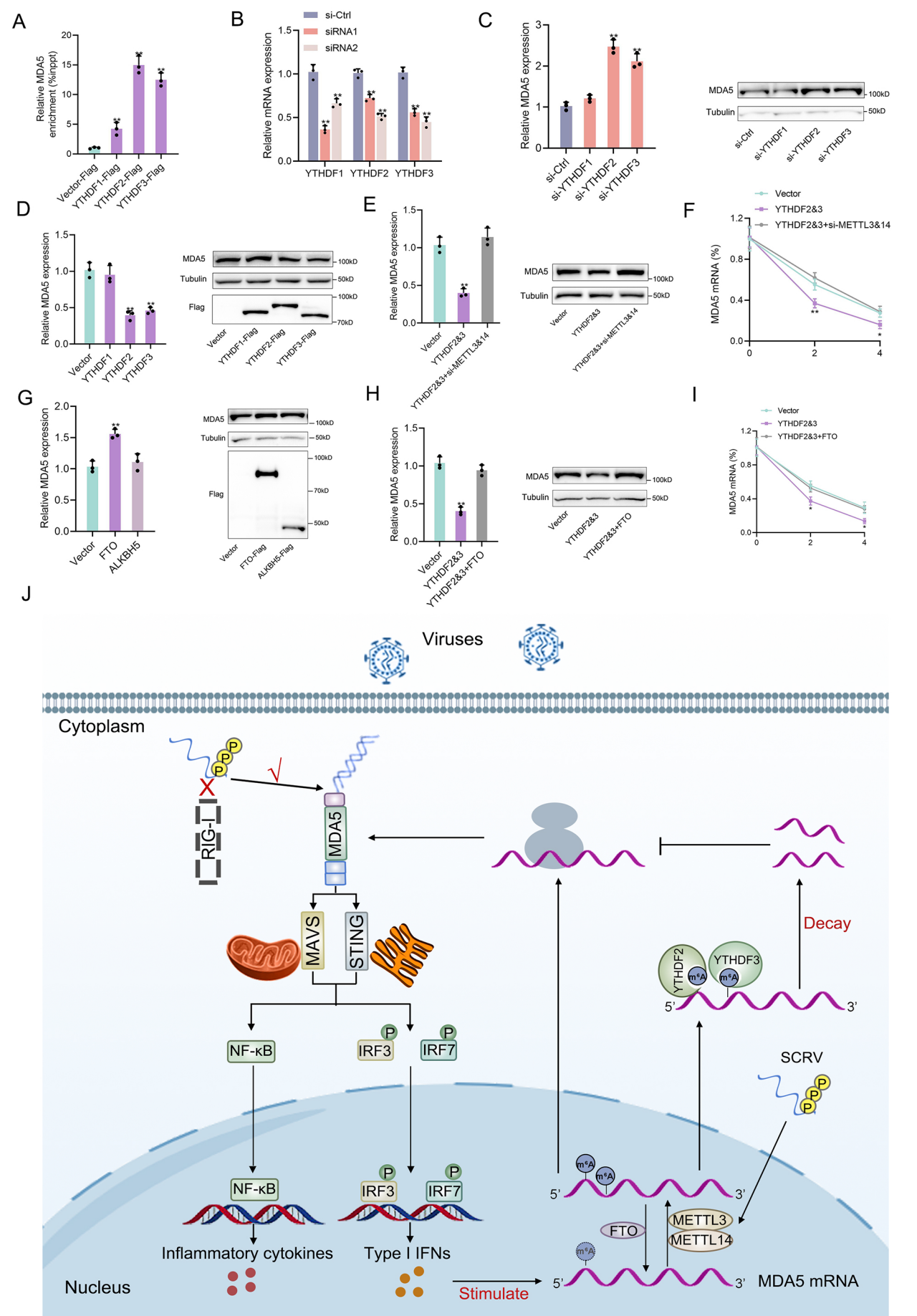
A
Relative MDA5 enrichment (%Input)
Vector-Flag
YTHDF1-Flag
YTHDF2-Flag
YTHDF3-Flag
B
si-Ctrl
siRNA1
siRNA2
Relative mRNA expression
YTHDF1
YTHDF2
YTHDF3
C
Relative MDA5 expression
si-Ctrl
si-YTHDF1
si-YTHDF2
si-YTHDF3
MDA5
Tubulin
100kD
50kD
D
Relative MDA5 expression
Vector
YTHDF1
YTHDF2
YTHDF3
Flag
70kD
E
Relative MDA5 expression
YTHDF2&3
YTHDF2&3+si-METTL3&14
F
Vector
YTHDF2&3
YTHDF2&3+si-METTL3&14
MDA5 mRNA (%)
G
Relative MDA5 expression
FTO
ALKBH5
FTO-Flag
ALKBH5-Flag
H
YTHDF2&3+FTO
I
YTHDF2&3+FTO
J
Viruses
Cytoplasm
RIG-I
MDA5
MAVS
STING
NF-κB
IRF3
IRF7
YTHDF2
YTHDF3
m6A
Decay
SCRV
METTL3
METTL14
FTO
Inflammatory cytokines
Type I IFNs
Nucleus
Stimulate
MDA5 mRNA